Zirconium in Rutile Thermometry: Temperature Estimates for Metamorphic Rocks of the Catalina Schist

Hollie McBride
GEOL 394
April 26, 2013
Advisors: Dr. Sarah Penniston-Dorland and Dr. Phil Piccoli

Table of Contents

Abstract

The Zr concentration of rutile grains was measured by EPMA for four metamorphic rock samples from the Catalina Schist. These samples include the garnet amphibolite core and actinolite schist rind of a single metasomatized amphibolite block, a garnet quartzite block, and a garnet blueschist block, all of which originate from mélange zones. The Zr in rutile thermometer calibrated by Tomkins et al. (2007) was used to obtain temperature estimates for each sample. At *P* = 1.0 GPa, the garnet amphibolite records a temperature range of 633 – 686 °C; the actinolite schist records a temperature range of 614 – 697 °C; the garnet quartzite records a temperature range of 648 – 708 °C, and the garnet blueschist records a temperature range of 567 – 601 °C, This is the first temperature estimate for garnet blueschist from the Catalina Schist. Statistical analyses show that there is no significant difference in the temperature recorded by the core and rind of the amphibolite block, indicating that the metasomatization of the block did not affect the concentration of Zr in rutile in the block as a whole. Although the amphibolite block and the garnet quartzite block originate from the same unit, the garnet quartzite records a higher temperature, which may reflect a differing metamorphic and tectonic history for different parts of the unit.

Introduction

The zirconium in rutile thermometer is based upon a reaction involving quartz (SiO_2), rutile (TiO_2), and zircon ($ZrSiO_4$): $ZrSiO_4 \rightleftharpoons ZrO_2(\text{in rutile}) + SiO_2$. Zirconium and titanium both have a 4+ oxidation state and a similar ionic radius (0.72Å and 0.61Å, respectively) and will readily substitute for each other within crystal sites. Previous research has shown that the solubility of ZrO_2 in rutile is strongly temperature dependent with solubility increasing with increasing temperature (Ferry and Watson, 2007; Tomkins et al., 2007; Watson et al., 2006; Zack et al., 2004).

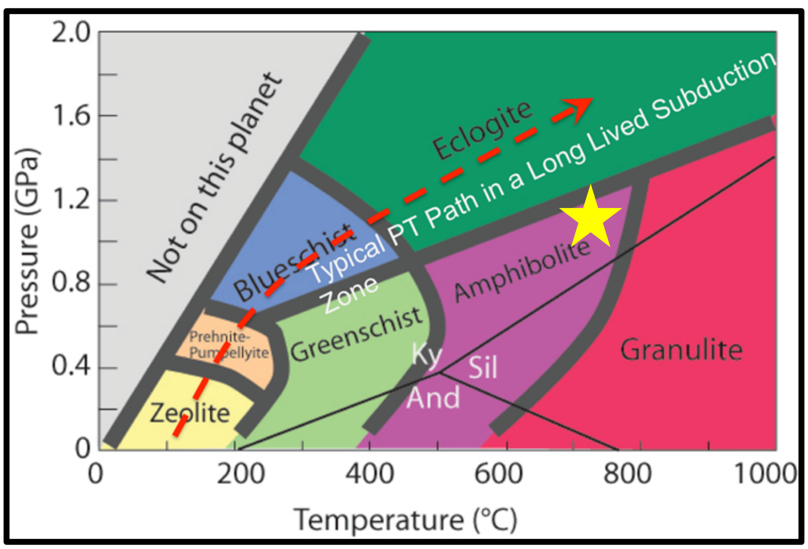

Figure 1: Pressure-temperature diagram illustrating metamorphic facies boundaries. Dashed red arrow indicates the typical *PT* path that subducted packages of rock follow in a long-lived subduction zone (i.e. blueschist to eclogite facies metamorphism). Yellow star denotes the location in *PT* space of the anomalously high temperature amphibolite units of the Catalina Schist (after Spear, 1993).

Zirconium in rutile is a nontraditional thermometer in that it is based on accessory phases as opposed to major phases. This invites further investigation into the use of other trace minerals in the field of thermobarometry. The Zr in rutile thermometer is also an important tool for geological research as a whole because it can be applied to a wide range of rock types due to the relatively common mineral assemblage quartz + rutile + zircon. Application of the thermometer to rocks of the Catalina Schist is significant because much of the thermometry for these rocks was performed with traditional thermobarometric techniques (Sorenson and Barton, 1987; Grove et al., 1995). It is prudent to apply a new thermometric technique to obtain updated temperature estimates.

The Catalina Schist is unique with respect to subduction zone complexes in general in that it is partially composed of high-temperature amphibolite-facies units (figure 1). Several models of the tectonic environment that might produce such high-grade assemblages have been proposed in the literature (Platt, 1975; Grove et al., 2008). Implications from temperature data are an important factor in the development of these models, thus a more accurate constraint on the temperatures conditions experienced by the Catalina Schist allows for informed interpretation of its tectonic history.

Geologic Setting

The Catalina Schist is a subduction-related metamorphic terrane located on Santa Catalina Island off the southern coast of California. It formed during the mid-Cretaceous and comprises five different metamorphic facies. In order of highest to lowest metamorphic grade, they are the amphibolite, albite-epidote amphibolite, epidote blueschist, lawsonite blueschist, and lawsonite-albite facies (figure 2). Both coherent and mélange-dominated units make up the Catalina Schist. These units are separated by a series of thrust faults (Platt, 1975).

Sorenson and Barton (1987) constrained the peak conditions of amphibolite facies metamorphism of the Catalina Schist to P = ~0.8-1.1 GPa and T = ~640-750 °C. They did so by applying traditional thermobarometric techniques to migmatitic, i.e. partially melted, amphibolite blocks from the mélange-dominated amphibolite unit. The techniques that were used include garnet-clinopyroxene thermometry and analysis of fluid inclusions. Grove and Bebout (1995) determined stability fields for all units of the Catalina Schist (figure 3). These stability fields are predicted based on thermodynamic data for the mineral assemblage found in each rock type.

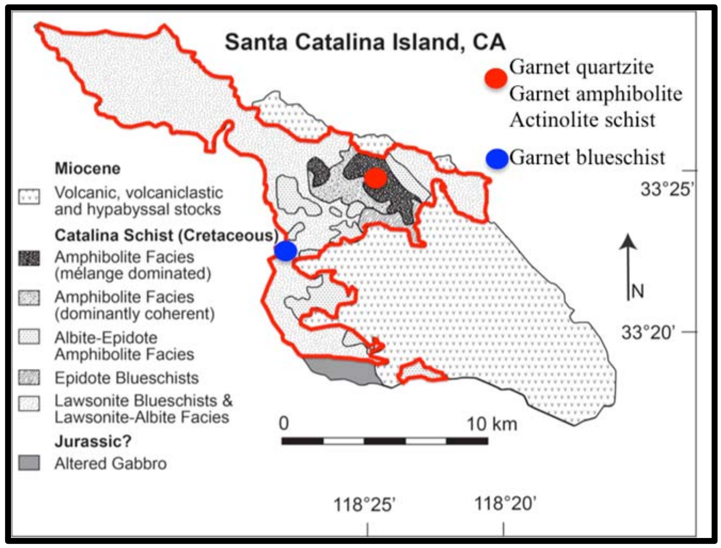

Figure 2: Geologic map of Santa Catalina Island outlining the different metamorphic facies present. Colored dots denote the units from which the four samples of this study originate (Grove and Bebout, 1995).

Rutile grains in four rock types from the Catalina Schist were analyzed in order to estimate the temperatures that they record. Three of these samples come from the mélange-dominated amphibolite unit. The mélange consists of meter- to kilometer- scale blocks of varying lithology suspended in a serpentinite matrix. One type of metamorphic block present is constructed of a garnet amphibolite core surrounded by an actinolite schist reaction rind (figure 4). Rutile from both the core (A10-3d) and the rind (A10-3a) were chosen for analysis in order to determine if they record the same temperature, as they compose a single block. The garnet quartzite block (A12A-5) originates from the same mélange-dominated amphibolite unit as the amphibolite block, but has a different lithology. It was selected for analysis in order to establish whether there is consistency in the temperature recorded by these two different blocks from the same mélange unit.

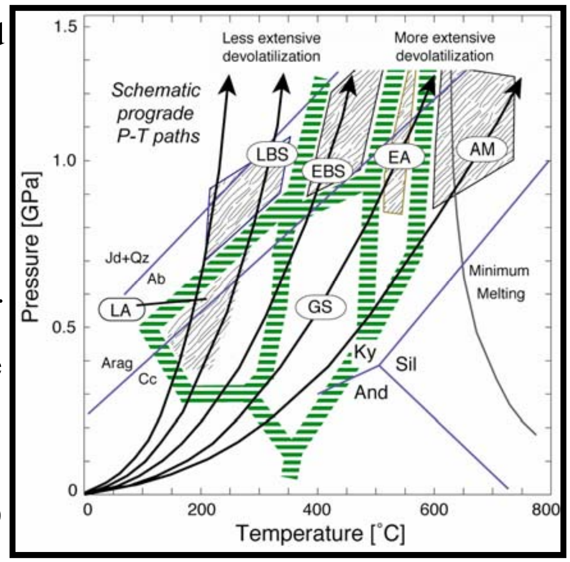

Figure 3: PT diagram showing stability fields for the different metamorphic facies of the Catalina Schist. AM: Amphibolite EA: Albite-Epidote Amphibolite EBS: Epidote Blueschist LBS: Lawsonite Blueschist LA: Lawsonite-Albite (Bebout, 2007).

The garnet blueschist block (GB12-1a) was chosen for analysis because, to date, no thermometry work has been performed on this particular lithology in the Catalina Schist. This study is the first to do so, and as such, makes an important contribution to the overall body of knowledge of the Catalina Schist. This block is located in the low-grade lawsonite blueschist unit. An additional reason this sample was selected for study was to determine whether or not it records a temperature consistent with the lawsonite blueschist stability field (figure 3).

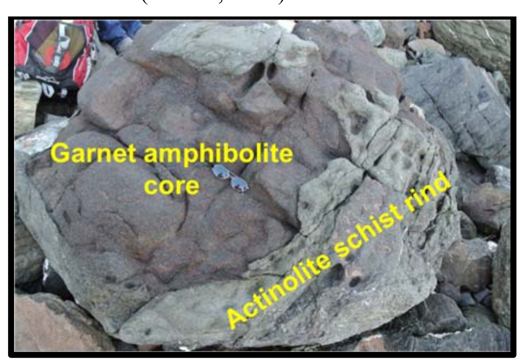

Figure 4: Field photograph of the amphibolite block that comprises a garnet amphibolite core (A10-3d) and actinolite schist reaction rind (A10-3a). Rutile grains in both the core and the rind were analyzed to determine whether or not this block as a whole records the same temperature. Photo credit: S. Penniston-Dorland

Zirconium in Rutile Thermometer

Several calibrations of the Zr in rutile thermometer have been derived over the course of the past decade. One of the first calibrations was empirical, and was developed by Zack et al. (2004). In their study, the authors measured the Zr content of rutile in 31 natural samples with previously published temperature estimates made by traditional thermometry techniques. An inherent problem with this approach is that the calibration can only be as accurate as the previous temperature estimates used to define it. Watson et al. (2006) developed a more refined thermometer by using synthetic samples in addition to natural samples. Subsequently, Ferry and Watson (2007) noted that in the absence of quartz, temperature estimates can still be made, provided that the activity of SiO_2 in quartz is known. In this study, temperature estimates for rocks from the Catalina Schist were made using the calibration of Tomkins et al. (2007), which takes into account the pressure dependence of Zr-Ti substitution. The calibration is $T(°C) = \frac{83.9+0.410P}{0.1428-Rln\phi}$ where P is pressure in kbar, R is the gas constant (0.0083144 kJ/K), and ϕ is Zr concentration in ppm. Values of 0.8 GPa, 0.9 GPa, 1.0 GPa, and 1.1 GPa will be used for P because the peak pressure conditions experienced by the Catalina Schist have been constrained to ~0.8-1.1 GPa (Sorenson and Barton, 1987).

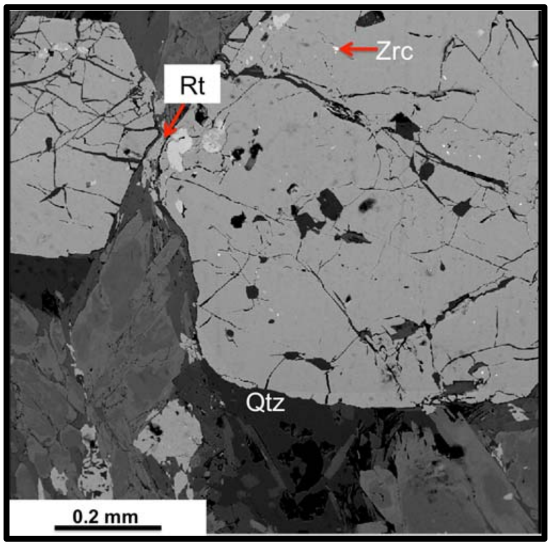

Figure 5: Back scattered electron image documenting the presence of rutile, zircon, and quartz in garnet blueschist.

Method of Analysis

The starting point for analysis of the four samples is to review the thin sections under a petrographic microscope. Mineral abundances and textural relationships are documented with photomicrographs. A principal goal of the petrographic characterization is to determine which rutile grains are best suited for analysis with the electron probe microanalyzer (EPMA). Considerations include size, crystal habit, alteration, location, and proximity to zircon and quartz. Once suitable grains have been identified, their location is noted on a thin section map. This map, in turn, is used to navigate to the grain and measure its zirconium concentration on the EPMA.

For each sample, it is essential to document the presence of the equilibrium mineral assemblage that defines the Zr in rutile thermometer, i.e. quartz, rutile, and zircon. Figures 5-8 demonstrate that all four samples contain this assemblage.

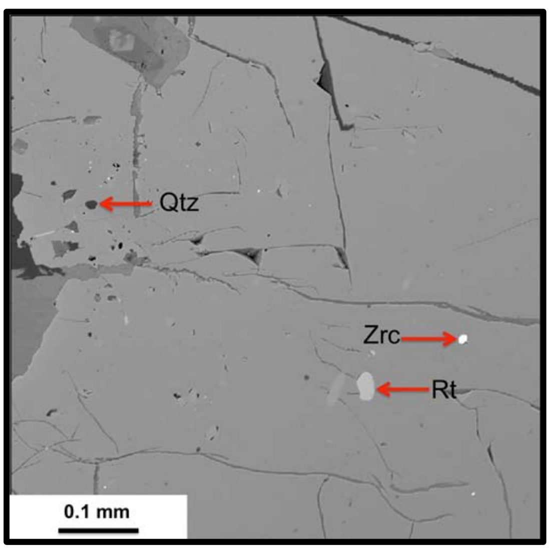

Figure 6: Back scattered electron image documenting the presence of rutile, zircon, and quartz in garnet amphibolite.

Under the guidance of Dr. Phil Piccoli, the probe used for this study was a JEOL JXA 8900R microanalyzer. The operating conditions were as follows: accelerating voltage of 20 kV, beam current of 120 nA, beam diameter of 5 μm, and counting times of 300s on the peak and 300s on the background. Synthetic crystals of TiO_2 and $ZrSiO_4$ were used as standards for Ti and Zr, respectively. The five WDS spectrometers were set up to measure the concentration of Ti, Zr, V, Fe, Cr, Al, and Si in rutile.

The concentration of Si is measured as a check to ensure that only rutile is being analyzed. Rutile is expected to have very low concentrations of Si. However, if a silicate phase such as zircon or garnet is unintentionally analyzed along with rutile, the Si concentration will be high. Following the protocol developed by Zack et al. (2004), analyses with Si concentrations greater than 300 ppm are excluded from further analysis.

Uncertainty

The uncertainties due to counting statistics on elemental concentrations measured with the EPMA are approximated by a modified version on the equation $1\sigma = \frac{\sqrt{N}}{N} \times 100$ where N is the number of X-ray counts detected by the probe for a given element. This relative uncertainty is reported in percent, but can be converted to absolute uncertainty in ppm.

For example: the concentration of Zr that was measured in grain number one during run number one in A10-3d was 321 ppm ± 5.47% (table 3). At the 1σ level, the absolute uncertainty for this measurement is 321 ppm × 0.0547, or 17.6 ppm. At the 2σ level, the uncertainty is 2 × 17.6 ppm, or 35.1 ppm. For each run, the uncertainty on Zr concentration can be used to define a range of temperatures calculated from the Zr in rutile thermometer. If the concentration of Zr in run #1 is 321 ± 35 ppm, then the corresponding temperature range is 637-655 °C. Lower and upper temperature estimates for ϕ = 321 – 35 ppm (i.e. 286 ppm) and ϕ = 321 + 35 ppm (i.e. 356 ppm) were calculated using the Tomkins et al. calibration (2007). This process was repeated for each run. See appendix A, table 3 for Zr concentration, relative uncertainty, absolute uncertainty, and corresponding temperature range for all rutile grains that were analyzed in A10-3d, A10-3a, A12A-5, and GB12-1a.

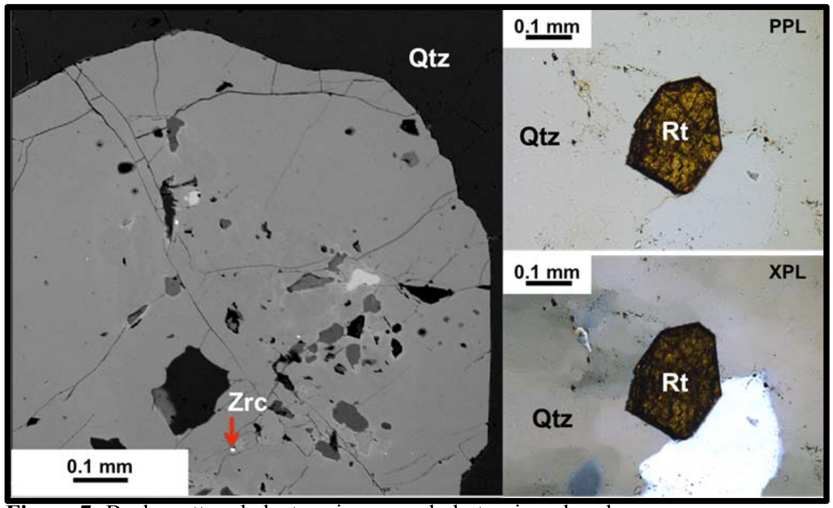

Figure 7: Back scattered electron image and photomicrophraphs documenting the presence of rutile, zircon, and quartz in garnet quartzite.

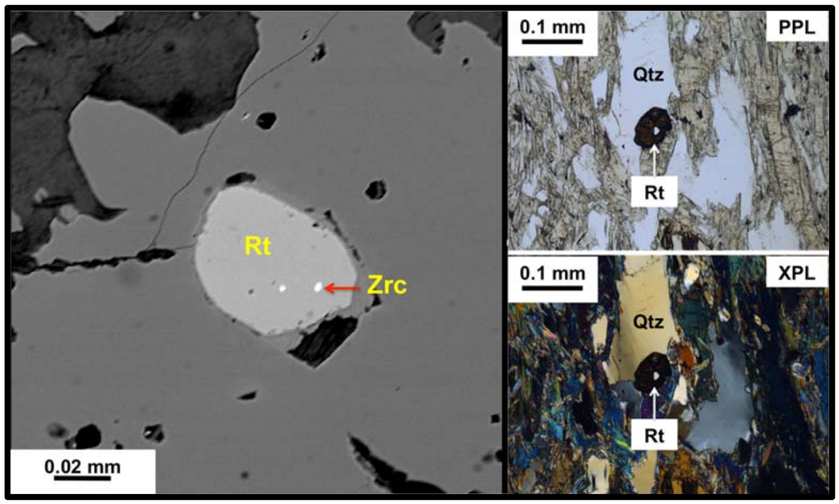

Figure 8: Back scattered electron image and photomicrophraphs documenting the presence of rutile, zircon, and quartz in actinolite schist.

Presentation of Data

A10-3d: Garnet Amphibolite Core

A total of 34 analyses were made on nine rutile grains in sample A10-3d (appendix B). The concentration of Zr in these grains ranges from 243 ± 35 ppm to 463 ± 46 ppm. The interquartile range of Zr concentration is 376 – 428 ppm, which represents a T range of range 668 - 679 °C at P = 1.0 GPa (figure 9). The absolute uncertainty on the Zr concentration was used to determine if any of the seven grains are heterogeneous with respect to their Zr concentration. If the lowest and highest Zr concentrations measured in each grain differ beyond the statistical uncertainty, then the grain has a heterogeneous Zr concentration. Of the eight grains upon which multiple analyses were performed, three are heterogeneous and four are homogenous;

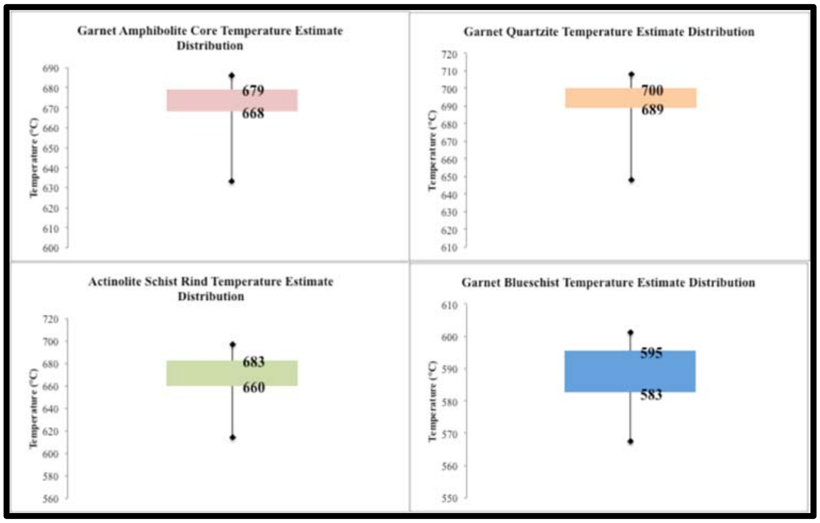

Figure 9: Boxplots showing the range of *T* recorded by each sample at *P* = 1.0 GPa. Lower tails represent the first quartile and upper tails represent the fourth quartile of the *T* range; colored boxes and corresponding data labels show the inter-quartile range.

grain 5a (appendix A, table 3) was only analyzed at one spot. Evidence for chemical zoning, i.e. a systematic increase or decrease in Zr concentration from the core to rim of a grain, is not present in any of the grains.

.

A10-3a: Actinolite Schist Rind

A total of 44 analyses were made on 11 rutile grains in A10-3a (appendix C). The concentration of Zr ranges from 190 ± 36 ppm – 526 ± 41 ppm, with an interquartile range of 340 – 447 ppm. This interquartile range corresponds to a *T* range of 660 – 683 °C for *P* = 1.0 GPa (figure 9). Five grains have a heterogeneous Zr concentration, four are homogenous, and one is chemically zoned from core to rim (appendix A, table 3, grain #7).

A12A-5: Garnet Quartzite

A total of 50 analyses were made on seven rutile grains in A12A-5 (appendix D). The concentration of Zr ranges from 294 ± 37 ppm – 594 ± 38 ppm with an interquartile range of 479 – 543 ppm. This interquartile range corresponds to a *T* range of 689 – 700 °C for *P* = 1.0 GPa (figure 9). Three of the seven grains are heterogeneous and four grains are homogenous. There is no evidence for chemical zoning in any of the seven grains.

GB12-1a: Garnet Blueschist

A total of 11 analyses were made on seven grains in GB12-1a (appendix E). The concentration of Zr ranges from 98 ± 36 ppm – 159 ± 36 ppm with an interquartile range of 122 – 147 ppm. This interquartile range corresponds to a *T* range of 583 – 595 °C for *P* = 1.0 GPa (figure 9). All seven grains are within analytical uncertainty of each other with respect to their Zr concentration, thus the rutile in GB12-1a as a whole is homogenous.

Possible Influence of Fe and Cr

In addition to Zr, Fe and Cr may also compete for the Ti crystal site within rutile. If this is the case, there will be systematic correlation between the concentration of Zr and Fe and/or Cr in rutile, i.e. the concentration of Zr will decrease with higher concentrations of Fe

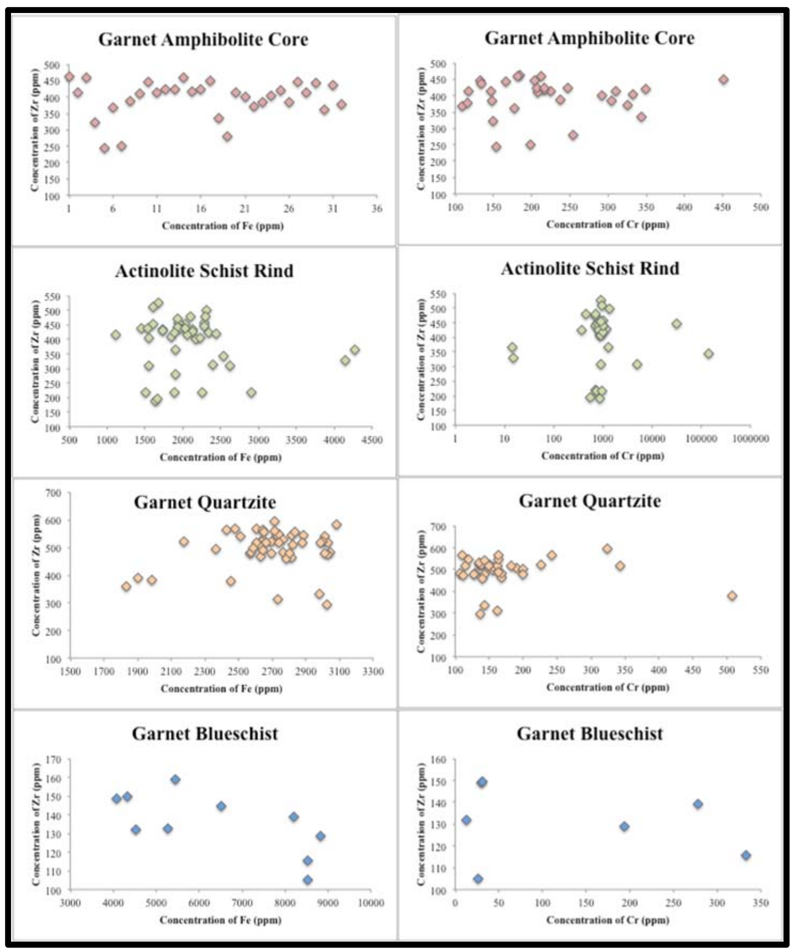

Figure 10: Plots of Cr concentration and Fe concentration vs. Zr concentration demonstrating that Cr and Fe do not exhibit an influence over Zr substitution in rutile.

and/or Cr. Figure 10 shows that for all four samples, there is no correlation between the concentration of Zr and Fe or Cr in the rutile grains that were analyzed.

Discussion of Results

	0.8 GPa	0.9 GPa	1.0 GPa	1.1 GPa
A10-3d	625-677 °C	629-681 °C	633-686 °C	637-690 °C
A10-3a	606-688 °C	610-693 °C	614-697 °C	618-702 °C
A12A-5	639-699 °C	644-704 °C	648-708 °C	652-713 °C
GB12-1a	560-593 °C	564-597 °C	567-601 °C	571-605 °C

Table 1: Range of temperature estimates calculated for the range of pea pressure conditions experienced by the Catalina Schist.

The temperature estimates that were calculated for each sample are dependent on pressure. The peak pressure conditions experienced by the Catalina Schist have been constrained to ~0.8-1.1 GPa (Sorenson and Barton, 1987). Table 1 displays the range of T calculated for this range of P. One goal of this study was to determine whether or not the core and rind of the amphibolite block and the garnet quartzite block from the same unit record the same temperature. The null hypothesis states that the samples do not record significantly different temperatures. In order to test this hypothesis, a statistical t test was used to determine if the mean temperature recorded by each of the four samples is significantly different from the mean temperature recorded by each of the other three samples.

The formula for this t test is $t = \frac{\overline{X}_1 - \overline{X}_2}{\sqrt{\left[\frac{(n_1-1)s_1^2+(n_2-1)s_2^2}{n_1+n_2-2}\right]\left[\frac{n_1+n_2}{n_1 n_2}\right]}}$ where $\overline{X}$ is the mean temperature of the sample, n is the total number of analyses performed on the sample, and s^2 is the variance, or the square of the standard deviation (1σ) for the temperature range of the sample; subscripts *1* and *2* refer to the two samples that are being compared (Salkind, 2007). If the calculated t value is less than the critical t value for rejection of the null hypothesis, then there is no significant difference between the respective temperature estimates. Table 2 displays the results of the t tests. See appendix A, table 4 for the data that were used for statistical analyses.

There is no significant difference between the temperatures recorded by the core (A10-3d) and the rind (A10-3a) of the single amphibolite block, which suggests that the metasomatism of the block had no affect on the Zr concentration of rutile in the block as a whole. There is a significant difference between the temperature recorded by the amphibolite block and the garnet quartzite block (A12A-5) despite the fact that they come from the same mélange-dominated amphibolite unit. This suggests that the amphibolite unit is not uniform in its metamorphic and tectonic history.

	A10-3d & A10-3a	A10-3d & A12A-5	A10-3d & GB12-1a	A10-3a & A12A-5	A10-3a & GB12-1a	A12A-5 & GB12-1a
t	0.54	6.41	18.79	5.85	11.73	23.78
Critical *t*	1.992	1.99	2.021	1.987	2.009	2.004
Reject H_0?	no	yes	yes	yes	yes	yes

Table 2: Results of t test for significant difference in temperature recorded by each sample. H_0 states that there will be no difference in temperature, thus rejection of H_0 indicates that t > critical t, thus the samples record significantly different temperatures. All samples record different temperatures with the exception of the garnet amphibolite and actinolite schist core and rind of the amphibolite block.

Another goal of the study was to determine if the garnet blueschist, which is found in the lawsonite blueschist unit, records a temperature consistent with the lawsonite blueschist stability field (figure 3). This stability field ranges from ~200-350 °C for the pressure conditions considered. The temperature estimates calculated for garnet blueschist (table 1) reveal that it experienced much hotter conditions.

Suggestions for Future Work

Temperature estimates play an integral role in deriving the metamorphic history of a rock, but they are not the only component. When thermometry is combined with barometry and chronology, the full pressure-temperature-time (*P-T-t*) path experienced by a metamorphic rock can be constructed. Recent advances in U-Pb dating of rutile present the exciting possibility of using chronology to date the rutile that was analyzed in this study (Zack et al., 2011).

Conclusions

The mineralogy and chemical composition of the amphibolite block have been altered by metasomatism resulting in a distinct garnet amphibolite core (A10-3d) and actinolite schist rind (A10-3a). Rutile grains from both the core and rind record the same temperature. This uniformity suggests that the mechanism responsible for the metasomatism evidenced in this block did not change the Zr concentration of rutile in the block as a whole. This amphibolite block comes the mélange-dominated amphibolite unit of the Catalina Schist, as does the garnet quartzite block (A12A-5). Although they are from the same mappable unit, these samples record different temperatures, with the garnet quartzite being the hotter of the two blocks. The disparity in temperature recorded by these two blocks may represent a difference in metamorphic and tectonic history of different parts of the amphibolite unit. The garnet blueschist block (GB12-1a) records the lowest and most statistically different temperature of the four samples that were analyzed in this study. Although it is found in the lawsonite blueschist unit, it records temperatures that exceed the stability field for lawsonite blueschist. This study presents the first temperature estimates for this lithology of the Catalina Schist.

Acknowledgements

I thank my advisors, Dr. Sarah Penniston-Dorland and Dr. Phil Piccoli, for their continued support and assistance with this project. I also thank Julia Gorman, Leigh Roble, and Natalie Sievers for their work on the Catalina Schist and all of their useful advice through each stage of senior thesis.

References

Bebout, G.E., 2007. Metamorphic chemical geodynamics of subduction zones. *Earth and Planetary Science Letters*, 260: 373-393.

Ferry, J.M., and Watson, E.B., 2007. New thermodynamic models and revised calibrations for the Ti-in-zircon and Zr-in-rutile thermometers. *Contrib Mineral Petrol,* DOI 10.1007/s00410-007-0201-0.

Grove, M., and Bebout, G.E., 1995. Cretaceous tectonic evolution of coastal southern California: Insights from the Catalina Schist. *Tectonics*, 14: 1290-1308.

Grove, M., Bebout, G.E., Jacobson, C.E., Barth, A.P., Kimbrough, D.L., King, R.L., Lovera, O.M., Mahoney, B.J., and Gehrels, G.E., 2008. The Catalina Schist: Evidence for middle Cretaceous subduction erosion of southwestern North America.

Platt, J.P., 1975. Metamorphic and deformational processes in the Franciscan complex, California: Some insights from the Catalina Schist terrane. *Geological Society of America Bulletin*, 86: 1337-1347.

Salkin, N.J., 2007. Statistics for people who (think they) hate statistics…the Excel edition: Thousand Oaks, CA, Sage Publications Inc., 402p.

Sorenson, S.S., and Barton, M.D., 1987. Metasomatism and partial melting in a subduction complex: Catalina Schist, southern California. *Geology*, 15:115-118.

Spear, F.S. (1993) Metamorphic phase equilibria and pressure-temperature-time paths: Washington, DC, Mineralogical Society of America, 799 p.

Spear, F.S., Wark, D.A., Cheney, J.T., Schumacher, J.C., and Watson, E.B., 2006. Zr-in-rutile thermometry in blueschists from Sifnos, Greece. *Contrib Mineral Petrol*, 152:375-385.

Tomkins, H.S., Powell, R., and Ellis, D.J., 2007. The pressure dependence of the zirconium-in-rutile thermometer. *Journal of Metamorphic Petrology*, 25: 703-713.

Watson, E.B., Wark, D.A., and Thomas, J.B., 2006. Crystallization thermometers for zircon and rutile. *Contrib Mineral Petrol*, 151: 413-433.

Zack, T., Moraes, R., and Kronz, A., 2004. Temperature dependence of Zr in rutile: empirical calibration of a rutile thermometer. *Contrib Mineral Petrol*, 148: 471-488.

Zack, T., Stockli, D.F., Luvizotto, G.L., Barth, M.G., Belousova, E., Wolfe, M.R., Hinton, R.W., 2011. In situ U–Pb rutile dating by LA-ICP-MS: ^{208}Pb correction and prospects for geological applications. *Contrib Mineral Petrol,* 165: 515-530.

Appendix A: Data Tables

	Grain No.	Run No.	Zr (ppm)	Cr (ppm)	Fe (ppm)	Si (ppm)	Zr Rel. Uncert. (%)	Zr 2σ Abs. Uncert. (ppm)	*T* (°C)								Sample#_Grain#_Relative Location
									***P* = 0.8 GPa**		***P* = 0.9 GPa**		***P* = 1.0 GPa**		***P* = 1.1 GPa**		
									Upper	**Lower**	**Upper**	**Lower**	**Upper**	**Lower**	**Upper**	**Lower**	
\	**1**	**8**	463	184	2647	2	5	46	685	668	690	673	694	677	699	681	A10-3D_1_Garnet Center
		9	415	117	3409	38	3.99	33	674	661	679	665	683	669	687	674	A10-3D_1_Garnet Center_Rutile Rim
		10	458	182	3022	23	4.49	41	684	668	688	673	693	677	697	681	A10-3D_1_Garnet Center_Rutile Rim
	2	**1**	321	149	*	0	5.47	35	655	637	659	642	664	646	668	650	A10-3D_2_Matrix
		2	243	154	*	29	7.28	35	635	613	639	617	644	621	648	625	A10-3D_2_Matrix
		23	369	109	3064	29	4.97	37	666	649	670	654	675	658	679	662	A10-3D_2_Matrix_Rutile Rim
		24	249	199	2700	0	7.16	36	637	615	641	619	646	623	650	627	A10-3D_2_Matrix_ Rutile Rim
	3a	**18**	389	237	4672	39	4.89	38	670	654	674	658	679	662	683	667	A10-3D_3a_Garnet Rim_Rutile Rim
		19	411	208	4238	20	4.75	39	675	658	679	663	683	667	688	672	A10-3D_3a_Garnet Rim_Rutile Center
		20	448	204	4351	9	4.52	40	682	666	686	671	691	675	695	679	A10-3D_3a_Garnet Rim_Rutile Center
		21	415	225	4301	0	4.1	34	674	660	679	665	683	669	688	674	A10-3D_3a_Garnet Rim_Rutile Center
		22	423	207	4454	6	4.43	38	677	662	681	666	686	670	690	675	A10-3D_3a_Garnet Rim_Rutile Rim
	3b	**31**	422	248	3838	67	4.4	37	676	661	681	666	685	670	690	675	A10-3D_3b_Garnet Rim_Rutile Rim
		32	460	212	3366	0	4.2	39	684	669	688	673	693	678	697	682	A10-3D_3b_Garnet Rim_Rutile Center
		33	416	217	3367	43	4.19	35	675	661	679	665	684	669	688	674	A10-3D_3b_Garnet Rim_Rutile Center
		34	425	216	3557	9	3.85	33	676	663	680	667	685	672	689	676	A10-3D_3b_Garnet Rim_Rutile Rim
	5a	**6**	451	451	4935	107	4.18	38	682	667	686	672	691	676	695	681	A10-3D_5a_Garnet Center
	5b	**3**	335	343	2269	27	5.42	36	658	641	663	645	667	649	671	654	A10-3D_5b_Garnet Rim_Rutile Center
		4	281	255	3025	36	6.38	36	645	625	650	629	654	634	658	638	A10-3D_5b_Garnet Rim_Rutile Rim
		12	415	310	3449	44	4.21	35	675	660	679	665	684	669	688	674	A10-3D_5b_Garnet Center_Rutile Rim
	6	**26**	402	292	3740	24	4.34	35	672	657	676	662	681	666	685	671	A10-3D_6_Garnet Rim_Rutile Rim
		27	370	326	3425	34	5.8	43	667	648	672	652	676	657	681	661	A10-3D_6_Garnet Rim_Rutile Center
		28	386	304	3214	48	4.57	35	669	654	673	658	678	662	682	667	A10-3D_6_Garnet Rim_Rutile Center
		29	403	333	3327	0	4.95	40	673	656	678	661	682	665	686	670	A10-3D_6_Garnet Rim_Rutile Center
		30	420	349	3620	24	4.77	40	677	660	681	665	685	669	690	674	A10-3D_6_Garnet Rim_Rutile Rim
	7	**13**	386	148	2838	86	4.73	37	681	667	685	671	690	676	694	680	A10-3D_7_Matrix_Rutile Rim
		14	447	133	2896	0	4.1	37	675	660	679	664	684	669	688	673	A10-3D_7_Matrix_Rutile Center

		15	415	147	2932	0	4.41	37	680	666	684	670	689	674	693	679	A10-3D_7_Matrix_Rutile Center
		16	442	166	2849	89	4.16	37	669	653	674	658	678	662	683	667	A10-3D_7_Matrix_Rutile Rim
	8	**7**	363	177	2751	0	4.1	30	663	649	667	654	672	658	676	662	A10-3D_8_Garnet Center
		11	438	134	4482	78	4.06	36	679	665	683	670	688	674	692	678	A10-3D_8_Garnet Center_Rutile Rim
		17	378	116	2292	49	4.42	33	667	652	671	656	676	661	680	665	A10-3D_8_Garnet Center_Rutile Rim
A10-3a	**1**	**101**	309	5016	2626	163	6.46	40	653	632	658	637	662	641	666	645	A10-3A_1_Matrix_Rutile Edge
		102	281	0	1905	36	6.51	37	646	625	650	629	654	633	659	638	A10-3A_1_Matrix_Rutile Center
		103	344	138656	2538	93	5.5	38	661	643	665	647	670	651	674	656	A10-3A_1_Matrix_Rutile Center
		104	218	0	2906	215	8.32	36	628	603	632	607	636	611	641	615	A10-3A_1_Matrix_Rutile Edge
	2	**105**	408	0	1841	126	4.55	37	674	658	678	663	683	667	687	671	A10-3A_2_Matrix_Rutile Edge
		106	433	1091	2128	31	4.33	38	678	664	683	668	687	672	692	677	A10-3A_2_Matrix_Rutile Center
		107	452	0	2026	19	4.15	38	682	667	686	672	691	676	695	681	A10-3A_2_Matrix_Rutile Center
		108	403	0	2169	107	4.63	37	673	657	677	662	682	666	686	670	A10-3A_2_Matrix_Rutile Edge
	3	**109**	365	1288	1897	58	5.09	37	665	648	669	653	674	657	678	661	A10-3A_3_Matrix_Rutile Edge
		110	427	1197	2131	82	4.41	38	677	662	682	667	686	671	691	675	A10-3A_3_Matrix_Rutile Center
		111	448	31454	1957	72	4.21	38	681	667	686	671	690	675	695	680	A10-3A_3_Matrix_Rutile Center
		112	457	1022	1940	129	4.48	41	683	668	688	672	692	677	697	681	A10-3A_3_Matrix_Rutile Edge
	4	**62**	478	442	2095	11	3.95	38	686	673	691	677	695	682	700	686	A10-3A_4_Matrix_Rutile Edge
		63	471	699	1929	16	4	38	685	671	690	676	694	680	699	685	A10-3A_4_Matrix_Rutile Center
		64	499	1349	2315	14	3.78	38	690	677	694	681	699	686	704	690	A10-3A_4_Matrix_Rutile Center
		65	458	0	2280	0	4.13	38	683	669	687	673	692	678	696	682	A10-3A_4_Matrix_Rutile Edge
	5	**81**	438	866	1445	127	4.28	37	679	665	684	669	688	674	693	678	A10-3A_5_Matrix_Rutile Edge
		82	526	916	1677	15	3.92	41	695	681	699	685	704	690	708	694	A10-3A_5_Matrix_Rutile Center
		83	436	768	1737	1	4.32	38	679	664	684	669	688	673	692	677	A10-3A_5_Matrix_Rutile Center
		84	431	957	1740	69	4.37	38	678	663	683	667	687	672	692	676	A10-3A_5_Matrix_Rutile Center
		85	440	814	1964	22	4.31	38	680	665	684	669	689	674	693	678	A10-3A_5_Matrix_Rutile Edge
	7	**76**	480	694	2301	57	3.97	38	687	673	691	677	696	682	700	686	A10-3A_7_Matrix_Rutile Edge
		77	447	751	2285	44	4.23	38	681	666	685	671	690	675	694	680	A10-3A_7_Matrix_Rutile Center
		78	219	695	2253	56	8.24	36	628	603	633	607	637	612	641	616	A10-3A_7_Matrix_Rutile Center
		79	216	753	1893	54	8.45	37	628	602	632	606	636	610	640	614	A10-3A_7_Matrix_Rutile Center
		80	441	718	1929	318	4.25	38									A10-3A_7_Matrix_Rutile Edge
	8	**66**	329	15	4144	122	5.6	37	657	639	662	643	666	647	670	652	A10-3A_8_Garnet Edge_Rutile Edge

		67	190	17929	3902	68	9.53	36									A10-3A_8_Garnet Edge_Rutile Center
		68	365	15	4272	99	5.12	37	665	648	669	653	674	657	678	661	A10-3A_8_Garnet Edge_Rutile Center
		69	291	0	6181	9005	6.34	37									A10-3A_8_Garnet Edge_Rutile Edge
	9	**70**	391	778	923	575	4.77	37									A10-3A_9_Matrix_Rutile Edge
		71	391	719	853	1788	4.77	37									A10-3A_9_Matrix_Rutile Center
		72	309	888	1548	32	5.93	37	653	633	657	638	661	642	666	646	A10-3A_9_Matrix_Rutile Center
		73	190	864	1630	0	9.47	36	619	591	623	595	627	599	632	603	A10-3A_9_Matrix_Rutile Center
		74	217	942	1511	75	8.33	36	628	602	632	607	636	611	640	615	A10-3A_9_Matrix_Rutile Center
		75	11984	109	10927	161223	0.39	93									A10-3A_9_Matrix_Rutile Edge
	11	**97**	315	0	2401	20	5.88	37	654	635	658	639	663	644	667	648	A10-3A_11_Matrix_Rutile Edge
		98	423	376	2342	52	4.46	38	677	661	681	666	686	670	690	675	A10-3A_11_Matrix_Rutile Center
		99	380	554	2375	6900	4.91	37									A10-3A_11_Matrix_Rutile Center
		100	251	781	2820	363	8.04	40									A10-3A_11_Matrix_Rutile Edge
	12	**86**	416	936	2054	21	4.49	37	675	660	680	664	684	669	689	673	A10-3A_12_Matrix_Rutile Edge
		87	421	875	2441	22	4.48	38	676	661	681	665	685	670	690	674	A10-3A_12_Matrix_Rutile Center
		88	405	858	2221	0	4.6	37	673	658	677	662	682	666	686	671	A10-3A_12_Matrix_Rutile Center
		89	440	825	2032	18	4.24	37	680	665	684	670	689	674	693	678	A10-3A_12_Matrix_Rutile Center
		90	424	841	1894	23	4.41	37	677	662	681	666	686	671	690	675	A10-3A_12_Matrix_Rutile Center
		91	406	901	1548	2	4.6	37	673	658	678	662	682	667	687	671	A10-3A_12_Matrix_Rutile Edge
	13	**92**	417	1002	1112	66	4.51	38	676	660	680	664	684	669	689	673	A10-3A_13_Matrix_Rutile Edge
		93	510	936	1608	40	3.75	38	692	679	696	683	701	688	705	692	A10-3A_13_Matrix_Rutile Center
		94	440	1030	1538	33	4.27	38	680	665	684	669	689	674	693	678	A10-3A_13_Matrix_Rutile Center
		95	452	921	1600	58	4.19	38	682	667	686	672	691	676	695	681	A10-3A_13_Matrix_Rutile Center
		96	195	562	1668	246	9.32	36	621	593	625	597	629	601	633	605	A10-3A_13_Matrix_Rutile Edge
A12A-5	**1**	**1**	495	156	2368	187	3.83	38	689	676	694	680	698	685	703	689	A12A-5_1_Matrix_Rut Edge
		2	523	139	2695	4	3.7	39	694	681	699	685	703	690	708	694	A12A-5_1_Matrix_Rut Center
		3	529	135	2643	53	3.64	38	695	682	699	686	704	691	708	695	A12A-5_1_Matrix_Rut Center
		4	479	144	2567	0	3.97	38	687	673	691	677	696	682	700	686	A12A-5_1_Matrix_Rut Center
		5	523	139	2638	0	3.67	38	694	681	698	685	703	690	707	694	A12A-5_1_Matrix_Rut Center
		6	505	190	2630	90	3.79	38	691	678	695	682	700	687	705	691	A12A-5_1_Matrix_Rut Edge
	2	**7**	531	135	2764	12	3.64	39	695	682	700	687	704	691	709	696	A12A-5_2_Matrix_Rut Edge
		8	483	129	2764	19	4	39	687	674	692	678	696	682	701	687	A12A-5_2_Matrix_Rut Center

		9	512	156	2823	27	3.78	39	692	679	697	683	701	688	706	692	A12A-5_2_Matrix_Rut Center
		10	520	151	3028	33	3.69	38	693	680	698	685	702	689	707	694	A12A-5_2_Matrix_Rut Center
		11	483	107	2574	46	3.94	38	687	674	692	678	696	682	701	687	A12A-5_2_Matrix_Rut Edge
		12	583	88	3081	18	3.27	38	703	691	708	696	712	700	717	705	A12A-5_2_Matrix_Rut Center
		13	540	143	3015	231	3.49	38	696	684	701	689	706	693	710	698	A12A-5_2_Matrix_Rut Center
		14	521	156	4665	18594	3.67	38									A12A-5_2_Matrix_Rut Center
		15	464	168	2815	79	4.09	38	684	670	689	674	693	679	698	683	A12A-5_2_Matrix_Rut Edge
		16	468	93	2629	125	4.05	38	685	671	689	675	694	680	698	684	A12A-5_2_Matrix_Rut Edge
		17	458	140	2785	0	4.16	38	683	669	688	673	692	678	697	682	A12A-5_2_Matrix_Rut Center
		18	312	162	2732	22	5.92	37	653	634	658	638	662	643	666	647	A12A-5_2_Matrix_Rut Center
		19	543	84	2886	30	3.52	38	697	685	702	689	706	694	711	698	A12A-5_2_Matrix_Rut Edge
		20	166290	0	2448	61914	0.09	299									A12A-5_2_Matrix_**Inclusion in Rutile**
		21	479	128	2804	55	3.95	38	687	673	691	677	696	682	700	686	A12A-5_3_Matrix_Rutile Edge
		22	523	226	2997	25	3.68	39	694	681	699	685	703	690	708	694	A12A-5_3_Matrix_Rutile Center
		23	482	168	3043	69	3.93	38	687	673	692	678	696	682	701	687	A12A-5_3_Matrix_Rutile Center
		24	517	161	2876	0	3.68	38	693	680	697	684	702	689	706	693	A12A-5_3_Matrix_Rutile Center
		25	474	112	3028	34	4	38	686	672	690	676	695	681	699	685	A12A-5_3_Matrix_Rutile Center
		26	294	136	3028	40	6.21	37	649	629	653	633	657	638	662	642	A12A-5_3_Matrix_Rutile Edge
	3	**27**	519	115	2664	68	3.69	38	693	680	698	685	702	689	707	694	A12A-5_3_Matrix_Rutile Edge
		28	519	183	2984	0	3.7	38	693	680	698	685	702	689	707	694	A12A-5_3_Matrix_Rutile Center
		29	545	164	2727	29	3.52	38	697	685	702	689	706	694	711	698	A12A-5_3_Matrix_Rutile Center
		30	480	98	3013	0	3.98	38	687	673	691	677	696	682	700	686	A12A-5_3_Matrix_Rutile Center
		31	333	144	2980	27	5.55	37	658	640	662	644	667	649	671	653	A12A-5_3_Matrix_Rutile Edge
		32	564	164	2430	240	3.41	38	700	688	705	693	709	697	714	702	A12A-5_3_Matrix_Rutile Edge
		33	568	109	2606	79	3.4	39	701	689	705	693	710	698	715	702	A12A-5_3_Matrix_Rutile Center
		34	548	119	2738	90	3.52	39	698	685	702	690	707	694	711	699	A12A-5_3_Matrix_Rutile Edge
		35	523	0	2176	257	3.6	38	694	681	698	686	703	690	707	695	A12A-5_4_Matrix_Rutile Edge
		36	566	242	2644	43	3.37	38	701	688	705	693	710	698	714	702	A12A-5_4_Matrix_Rutile Center
	4	**37**	594	325	2716	11	3.23	38	705	693	709	698	714	702	718	707	A12A-5_4_Matrix_Rutile Center
		38	560	75	2712	20	3.41	38	700	687	704	692	709	696	713	701	A12A-5_4_Matrix_Rutile Center
		39	541	83	2510	85	3.51	38	697	684	701	689	706	693	710	698	A12A-5_4_Matrix_Rutile Edge
	5	**40**	380	507	2452	83	4.82	37	668	652	672	656	677	661	681	665	A12A-5_5_Matrix_Rutile Edge

		41	546	70	2818	21	3.49	38	697	685	702	689	706	694	711	698	A12A-5_5_Matrix_Rutile Center
		42	557	98	2832	0	3.42	38	699	687	704	691	708	696	713	700	A12A-5_5_Matrix_Rutile Center
		43	519	343	2608	33	3.64	38	693	680	698	685	702	689	707	694	A12A-5_5_Matrix_Rutile Center
		44	570	0	2481	5	3.32	38	701	689	706	694	710	698	715	703	A12A-5_5_Matrix_Rutile Center
		45	555	0	2648	0	3.4	38	699	687	703	691	708	696	712	700	A12A-5_5_Matrix_Rutile Edge
	6	**53**	383	0	1983	268	4.86	37	669	652	673	657	678	661	682	666	A12A-5_6_Matrix_Rutile Edge
		54	359	55	1833	165	5.14	37	664	647	668	651	673	655	677	660	A12A-5_6_Matrix_Rutile Center
		55	389	0	1902	220	4.71	37	670	654	674	659	679	663	683	667	A12A-5_6_Matrix_Rutile Center
		56	399	0	1756	1273	4.57	36									A12A-5_6_Matrix_Rutile Edge
	7	**57**	505	147	2520	635	3.78	38									A12A-5_7_Matrix_Rutile Edge
		58	519	149	2737	187	3.68	38	693	680	698	685	702	689	707	694	A12A-5_7_Matrix_Rutile Center
		59	500	200	2585	202	3.81	38	690	677	695	681	699	686	704	690	A12A-5_7_Matrix_Rutile Center
		60	480	200	2693	257	3.97	38	687	673	691	677	696	682	700	686	A12A-5_7_Matrix_Rutile Center
		61	489	164	2645	528	3.89	38	688	675	693	679	697	684	702	688	A12A-5_7_Matrix_Rutile Edge
	8	**49**	195	0	3887	63499	9.46	37									A12A-5_8_Garnet Center_Rutile Center
	9	**46**	288	0	6085	2347	6.58	38									A12A-5_9_Garnet Center_Rutile Edge
		47	226	28	5225	4868	8.37	38									A12A-5_9_Garnet Center_Rutile Center
		48	56	0	175108	162951	36.52	41									A12A-5_9_Garnet Center_Rutile Edge
	10	**50**	0	13694	16319	36836	100	0									A12A-5_10_Garnet Center_Rutile Edge
		51	24	0	83101	59957	75.83	36									A12A-5_10_Garnet Center_Rutile Center
		52	0	141317	31441	31197	100	0									A12A-5_10_Garnet Center_Rutile Edge
GB12-1a	**1**	**1**	115	333	8528	109	15.13	35	589	547	593	551	597	555	601	559	GB12-1a_1_Rutile Rim_Garnet Center
		2	139	278	8216	55	12.55	35	600	564	604	568	608	572	612	576	GB12-1a_1_Rutile Center_Garnet Center
		3	81	0	113646	88504	22.93	37									GB12-1a_1_Rutile Edge_Garnet Edge
	2	**4**	103	0	50663	33657	17.42	36									GB12-1a_2_Rutile Edge_Garnet Center
		5	144	0	10272	1771	12.03	35									GB12-1a_2_Rutile Center_Garnet Center
	3	**18**	132	13	4526	18	13.68	36	597	558	601	562	605	566	609	570	GBS12-1a_3_gt edge_rut edge
		19	149	30	4070	172	12.06	36	604	569	608	573	612	577	616	581	GBS12-1a_3_gt edge_rut ctr
		20	150	31	4341	136	12.03	36	604	570	608	574	613	578	617	582	GBS12-1a_3_gt edge_rut edge
	5	**15**	118	153	15363	3875	15.1	36									GBS12-1a_5_gt ctr_rut ctr
	5a	**16**	132	146	12429	3197	13.55	36									GBS12-1a_5a_gt ctr_rut ctr

	10	**9**	129	0	8834	256	13.97	36	596	556	600	560	604	564	608	568	GBS12-1a_10_gt edge_rut edge
		10	105	0	8535	287	16.98	36	585	537	589	541	593	545	597	549	GBS12-1a_10_gt edge_rut ctr
		11	141	0	8665	1115	12.64	36									GBS12-1a_10_gt edge_rut ctr
	12	**28**	112	0	6499	2727	15.85	35									GBS12-1a_12_gt ctr_rut edge
	13	**29**	144	0	6508	112	12.41	36	602	567	606	570	610	574	615	578	GBS12-1a_13_gt ctr_rut ctr
	14	**30**	98	194	7543	277	18.31	36	581	530	585	534	589	538	593	542	GBS12-1a_14_host edge_rut ctr
	15	**32**	159	26	5450	257	11.21	36	608	575	612	579	616	583	620	587	GBS12-1a_15_gt edge_rut ctr
	16	**33**	133	0	5275	265	13.49	36	597	559	601	563	605	567	610	571	GBS12-1a_16_gt ctr_rut ctr

Table 3: Results of all EPMA analyses and thermometer calculations for the peak pressure conditions experienced by the Catalina Schist as constrained by Sorenson and Barton (1987). Samples are coded by color: red = garnet amphibolite core (A10-3d); green = actinolite schist rind (A10-3a); orange = garnet quartzite (A12A-5), and blue = garnet blueschist (GB12-1a). Grey rows denote EPMA runs that were excluded from further analysis due to concentration of Si > 300 ppm. *Not measured

Appendix A: Data Tables

Sample	Grain No.	Run No.	Zr (ppm)	T (°C) @ 1.0 GPa
A10-3d	1	8	463	686
		9	415	677
		10	458	685
	2	1	321	655
		2	243	633
		23	369	667
		24	249	635
	3a	18	389	671
		19	411	676
		20	448	683
		21	415	677
		22	423	678
	3b	31	422	678
		32	460	685
		33	416	677
		34	425	679
	5a	6	451	684
	5b	3	335	659
		4	281	644
		12	415	677
	6	26	402	674
		27	370	667
		28	386	670
		29	403	674
		30	420	678
	7	13	386	670
		14	447	683
		15	415	677
		16	442	682
	8	7	363	665
		11	438	681
		17	378	669
			Mean	672
			Std Dev	13
			Variance	181
			n	32

Sample	Grain No.	Run No.	Zr (ppm)	T (°C) @ 1.0 GPa
A10-3a	1	101	309	652
		102	281	644
		103	344	661
		104	218	625
	2	105	408	675
		106	433	680
		107	452	684
		108	403	674
	3	109	365	666
		110	427	679
		111	448	683
		112	457	685
	4	62	478	689
		63	471	687
		64	499	692
		65	458	685
	5	81	438	681
		82	526	697
		83	436	681
		84	431	680
		85	440	682
	7	76	480	689
		77	447	683
		78	219	625
		79	216	624
		80	441	682
	8	66	329	657
		68	365	666
	9	72	309	652
		73	190	614
		74	217	624
	11	97	315	654
		98	423	678
	12	86	416	677
		87	421	678
		88	405	674
		89	440	682
		90	424	678
		91	406	675
	13	92	417	677
		93	510	694
		94	440	682
		95	452	684
		96	195	616
			Mean	669
			Std Dev	22
			Variance	501
			n	44

Sample	Grain No.	Run No.	Zr (ppm)	T (°C) @ 1.0 GPa
A12A-5	1	1	495	692
		2	523	697
		3	529	698
		4	479	689
		5	523	697
		6	505	694
	2	7	531	698
		8	483	690
		9	512	695
		10	520	696
		11	483	690
		12	583	706
		13	540	699
		15	464	686
		16	468	687
		17	458	685
		18	312	653
		19	543	700
	3	21	479	689
		22	523	697
		23	482	689
		24	517	696
		25	474	688
		26	294	648
		27	519	696
		28	519	696
		29	545	700
		30	480	689
		31	333	658
		32	564	703
		33	568	704
		34	548	701
	4	35	523	697
		36	566	704
		37	594	708
		38	560	703
		39	541	700
	5	40	380	669
		41	546	700
		42	557	702
		43	519	696
		44	570	704
		45	555	702
	6	53	383	670
		54	359	664
		55	389	671
	7	58	519	696
		59	500	693
		60	480	689
		61	489	691
			Mean	691
			Std Dev	14
			Variance	184
			n	50

Sample	Grain No.	Run No.	Zr (ppm)	T (°C) @ 1.0 GPa
GB12-1a	**1**	**1**	115	579
		2	139	592
	3	**18**	132	588
		19	149	597
		20	150	597
	10	**9**	129	586
		10	105	572
	13	**29**	144	594
	14	**30**	98	567
	15	**32**	159	601
	16	**33**	133	588
			Mean	587
			Std Dev	11
			Variance	113
			n	11

Table 4: Median Zr concentration (with respect to the range defined by analytical uncertainty) and corresponding temperature at $P = 1.0$ GPa. These data were used to perform a t test in order to determine whether the temperature recorded by a given sample is significantly different from the temperature recorded by each of the other three samples.

Appendix B: Garnet Amphibolite Core

Figure 11: Thin section map of garnet amphibolite core (A10-3d) showing location of the nine rutile grains analyzed as denoted by stars. Numbers denote grain number, and correspond to grain number in tables 3 and 4, as well grain number in the following photomicrographs.

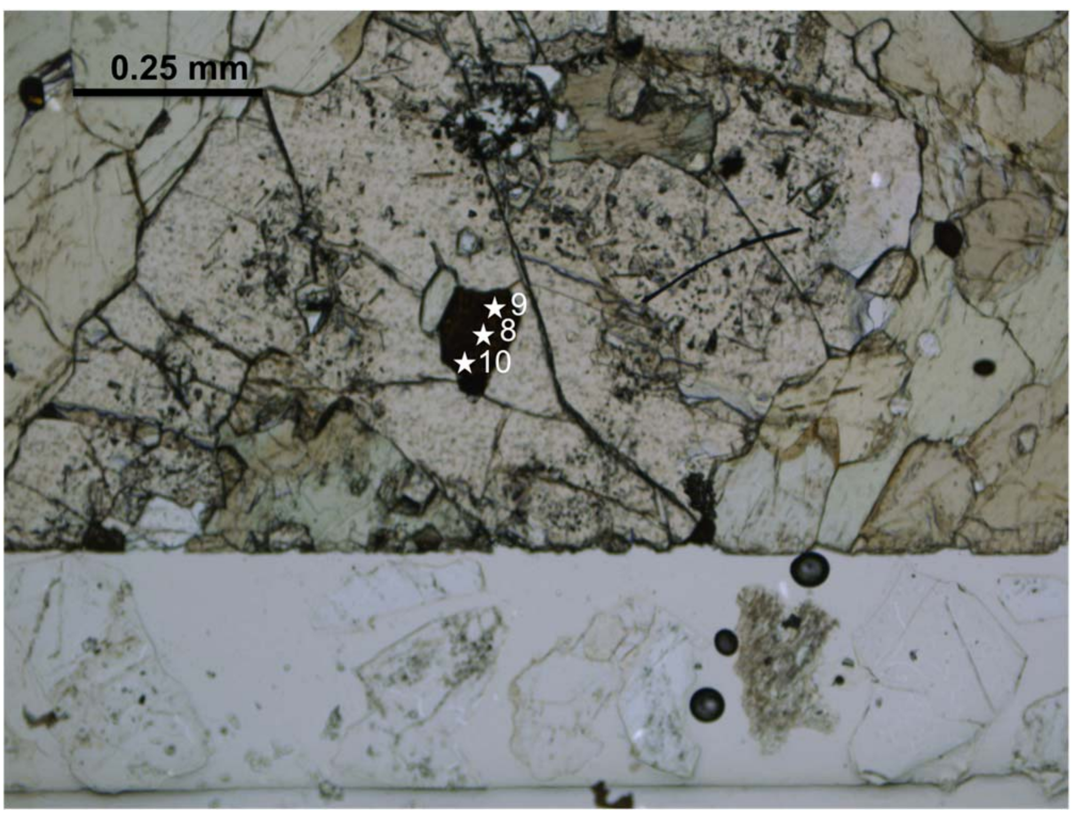

Figure 12: Rutile grain #1 from garnet amphibolite core (A10-3d). Stars denote EPMA run number.

Appendix B: Garnet Amphibolite Core

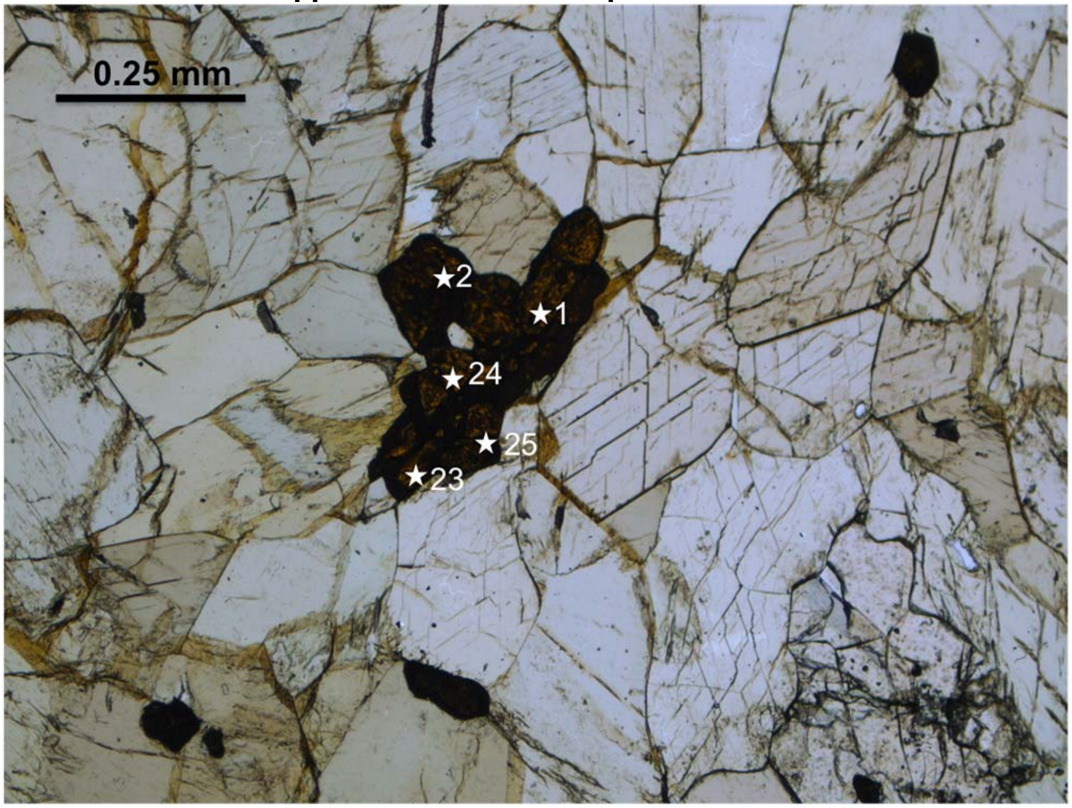

Figure 13: Rutile grain #2 from garnet amphibolite core (A10-3d). Stars denote EPMA run number.

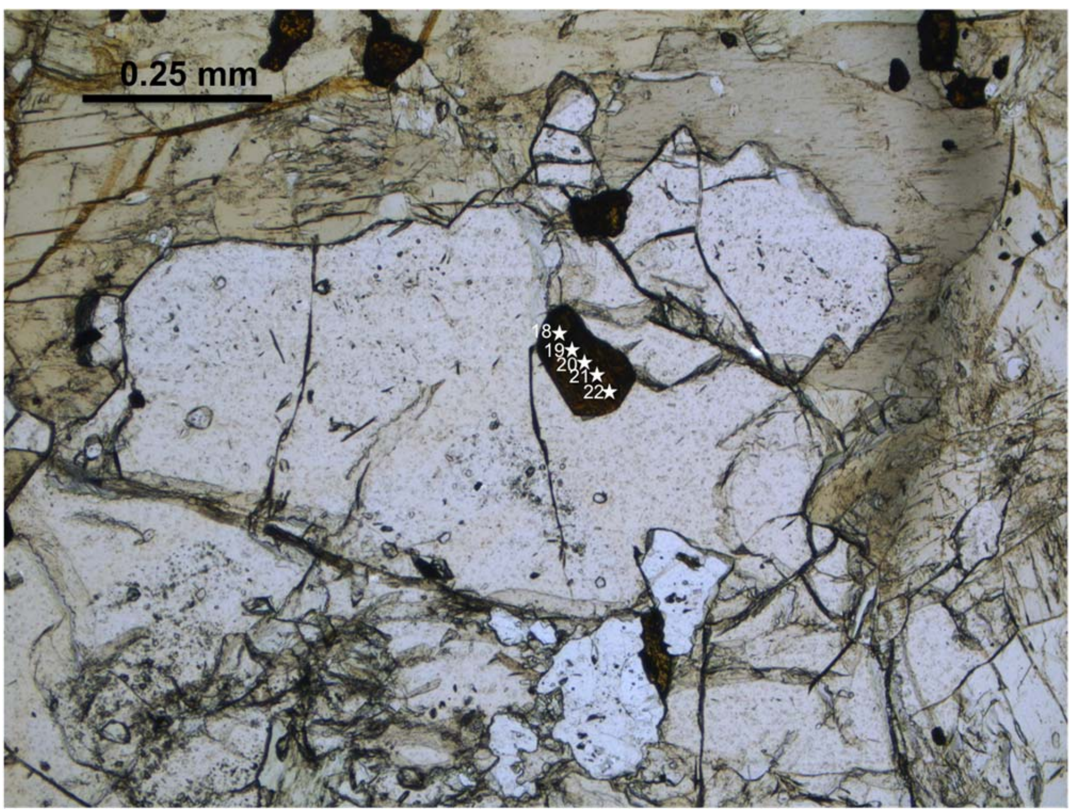

Figure 14: Rutile grain #3a from garnet amphibolite core (A10-3d). Stars denote EPMA run number.

Appendix B: Garnet Amphibolite Core

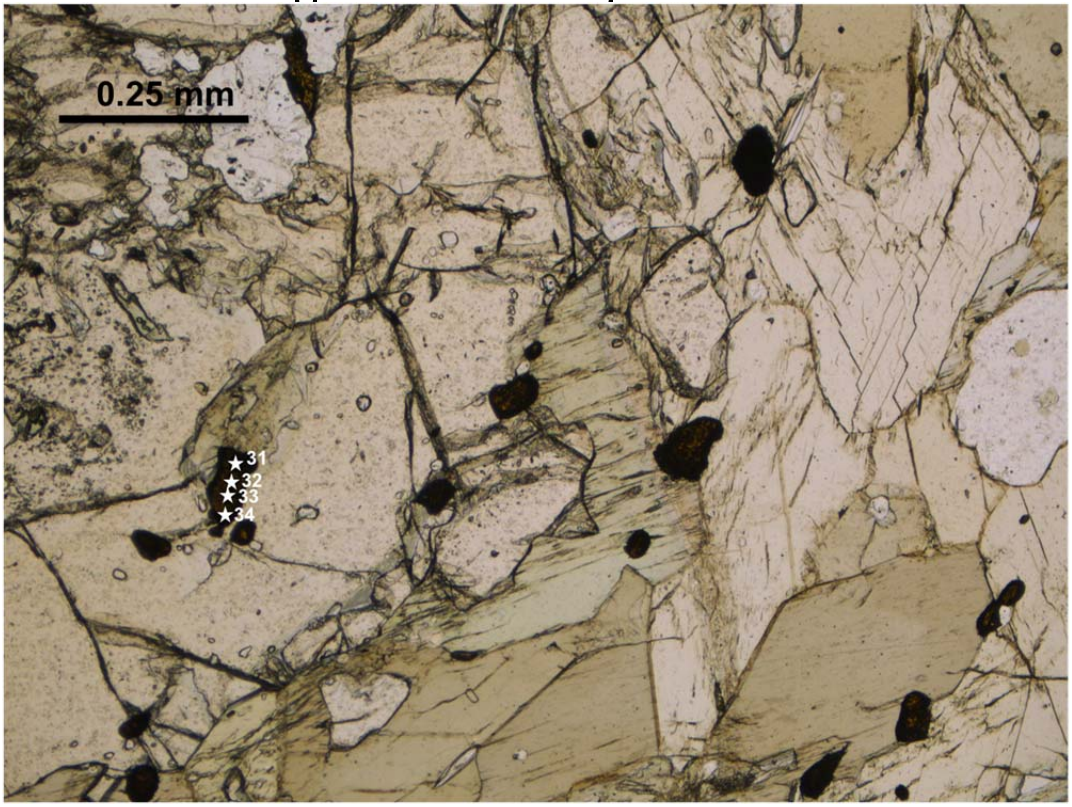

Figure 15: Rutile grain #3b from garnet amphibolite core (A10-3d). Stars denote EPMA run number.

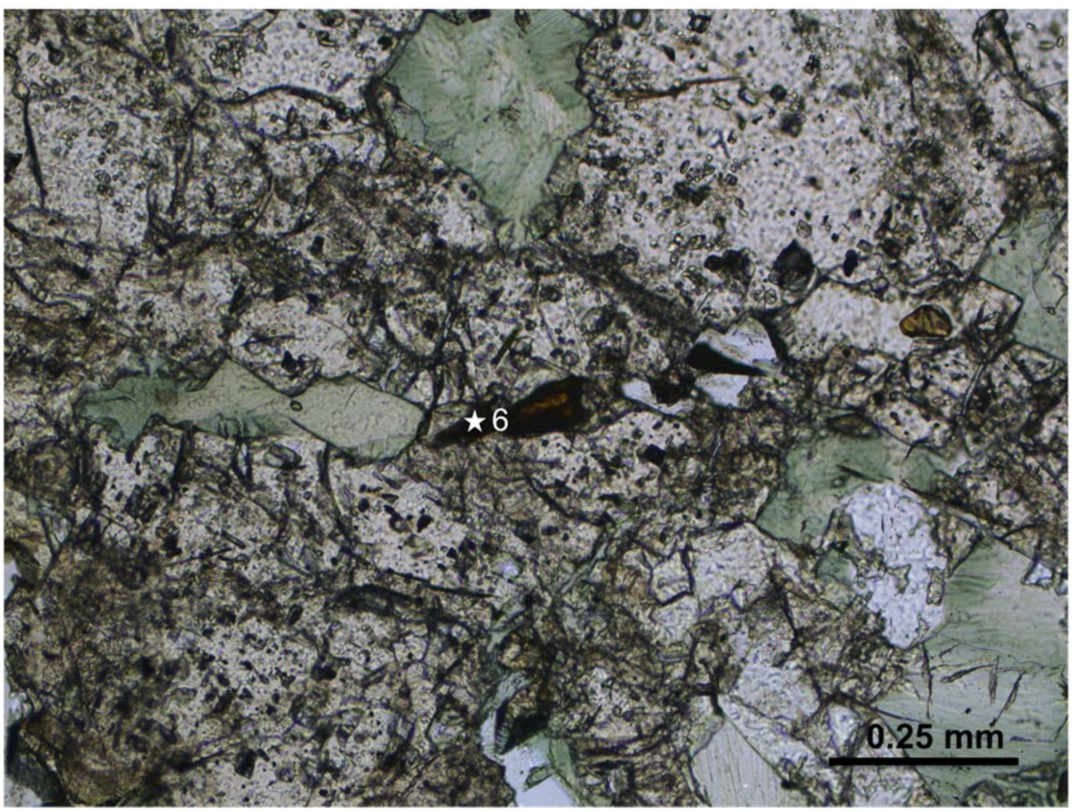

Figure 16: Rutile grain #5a from garnet amphibolite core (A10-3d). Star denotes EPMA run number.

Appendix B: Garnet Amphibolite Core

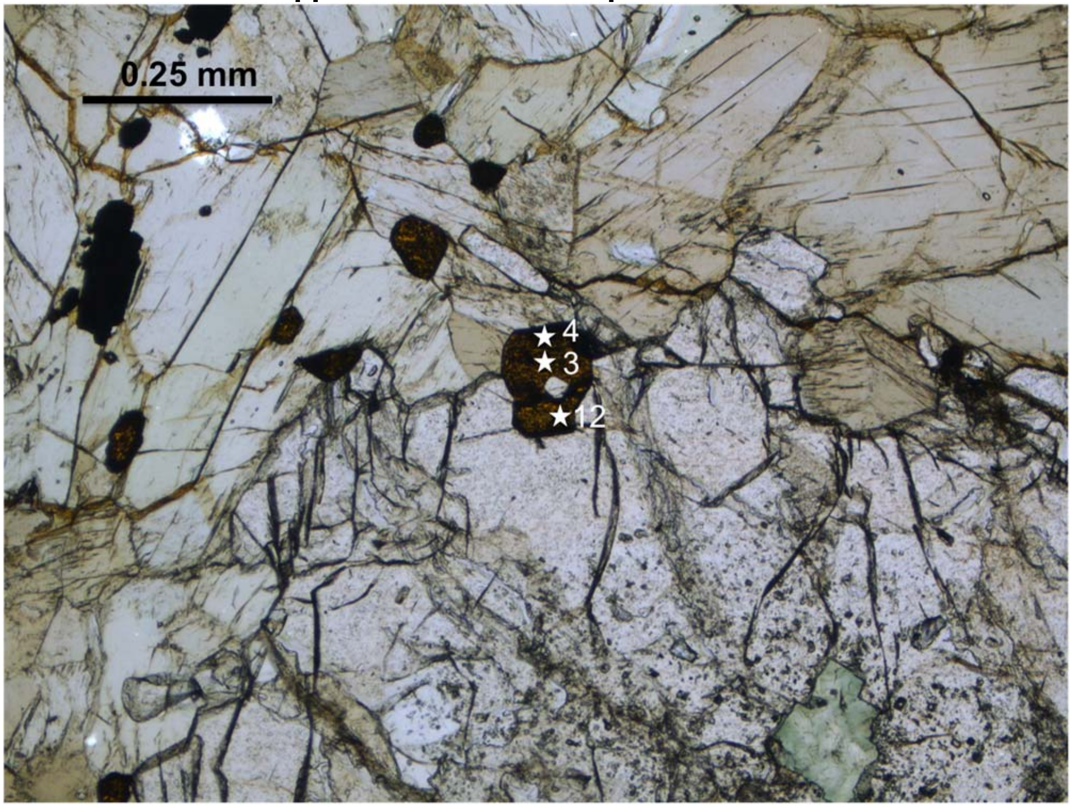

Figure 17: Rutile grain #5b from garnet amphibolite core (A10-3d). Stars denote EPMA run number.

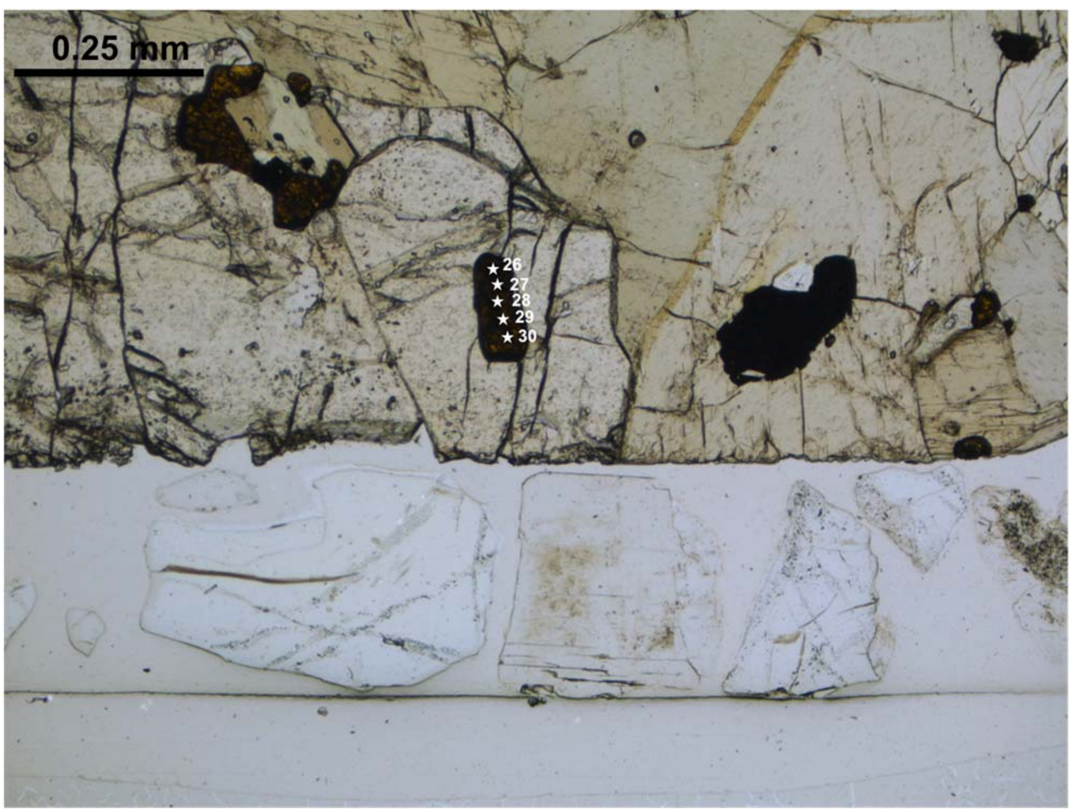

Figure 18: Rutile grain #5b from garnet amphibolite core (A10-3d). Stars denote EPMA run number.

Appendix B: Garnet Amphibolite Core

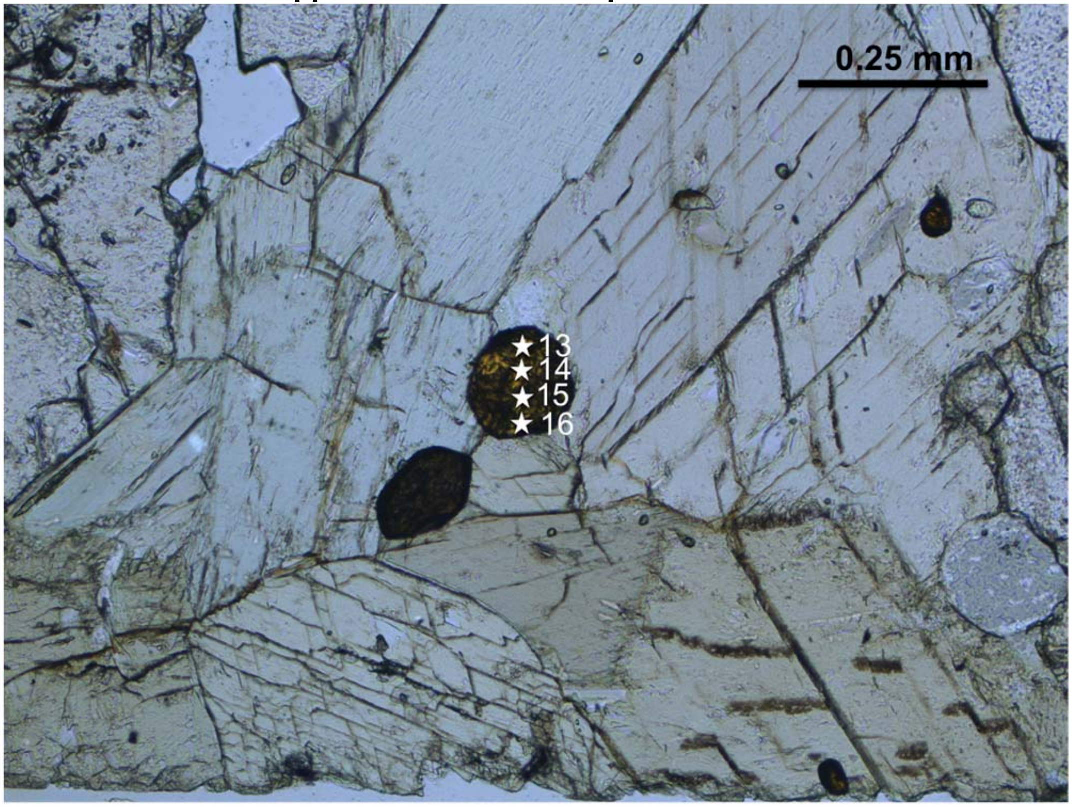

Figure 19: Rutile grain #7 from garnet amphibolite core (A10-3d). Stars denote EPMA run number.

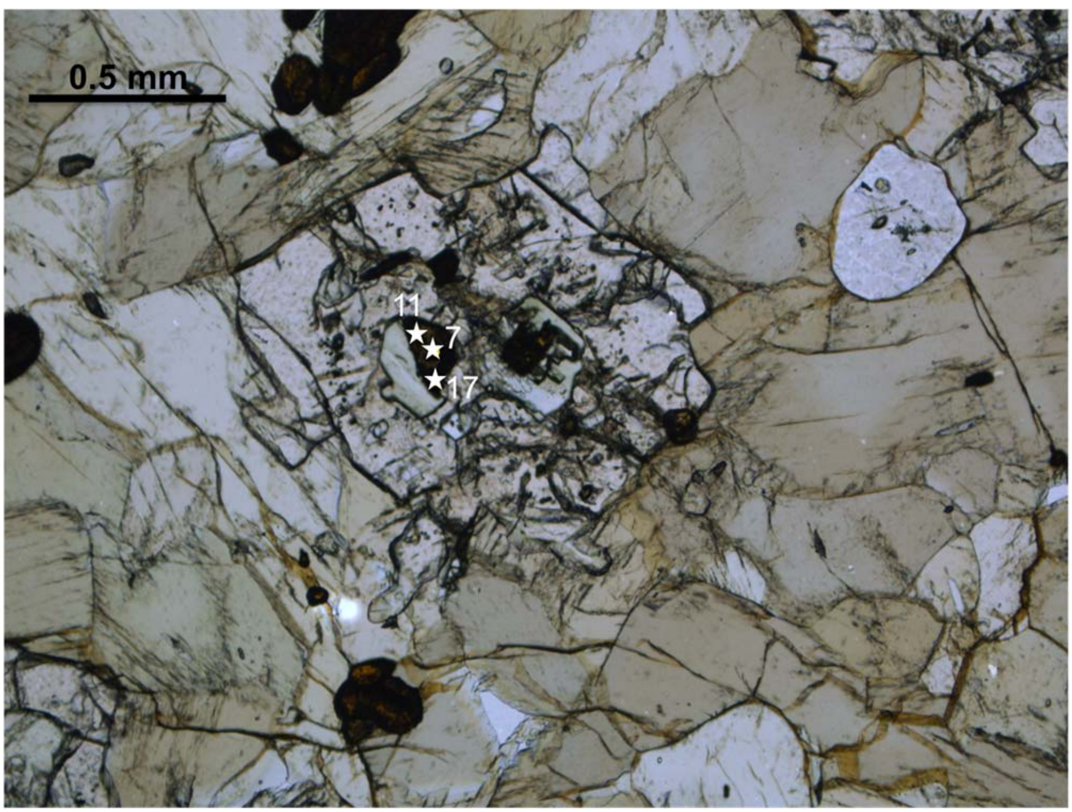

Figure 20: Rutile grain #8 from garnet amphibolite core (A10-3d). Stars denote EPMA run number.

Appendix C: Actinolite Schist Rind

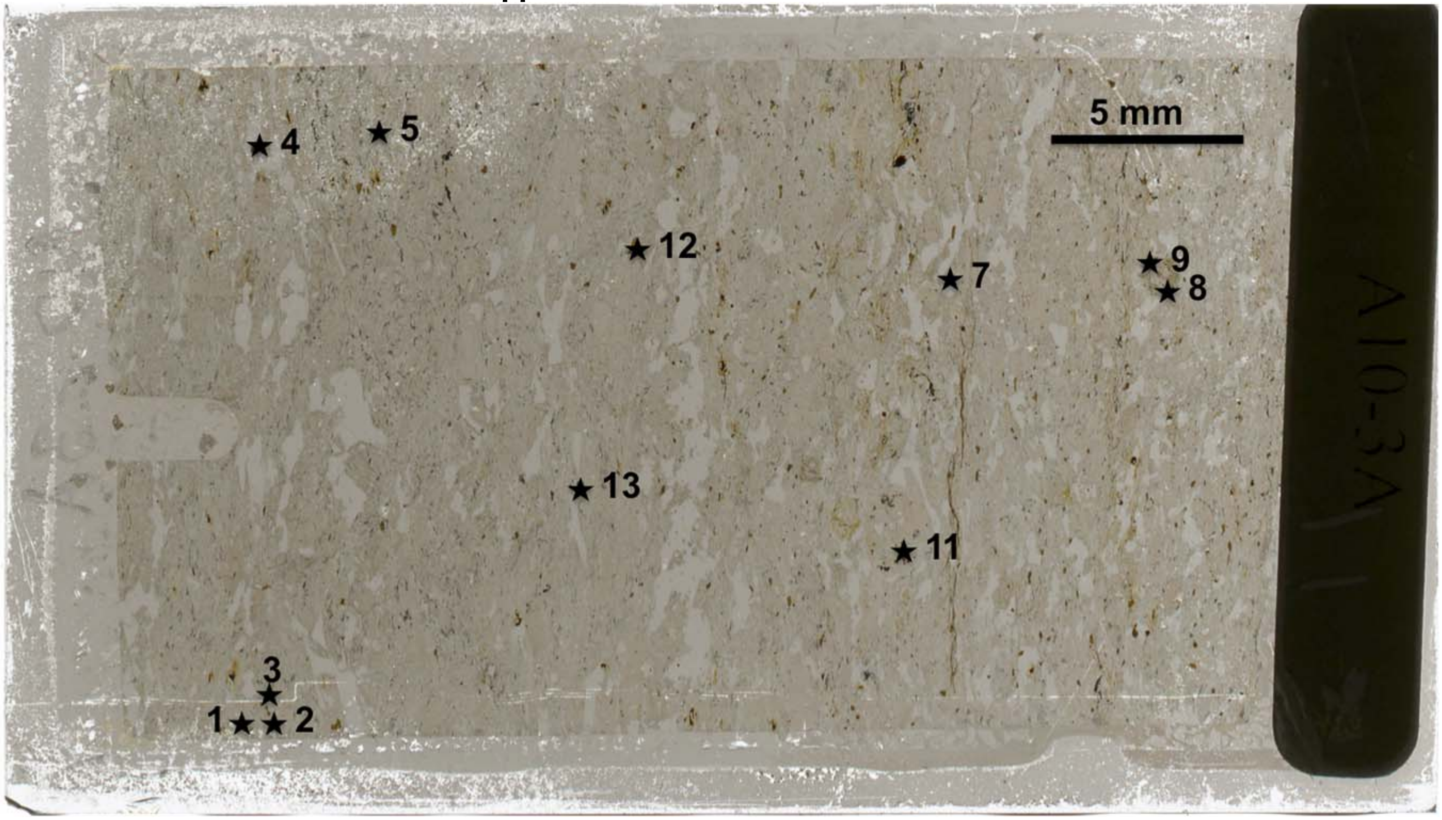

Figure 21: Thin section map of actinolite schist rind (A10-3a) showing location of the eleven rutile grains analyzed as denoted by stars. Numbers denote grain number, and correspond to grain number in tables 3 and 4, as well grain number in the following photomicrographs.

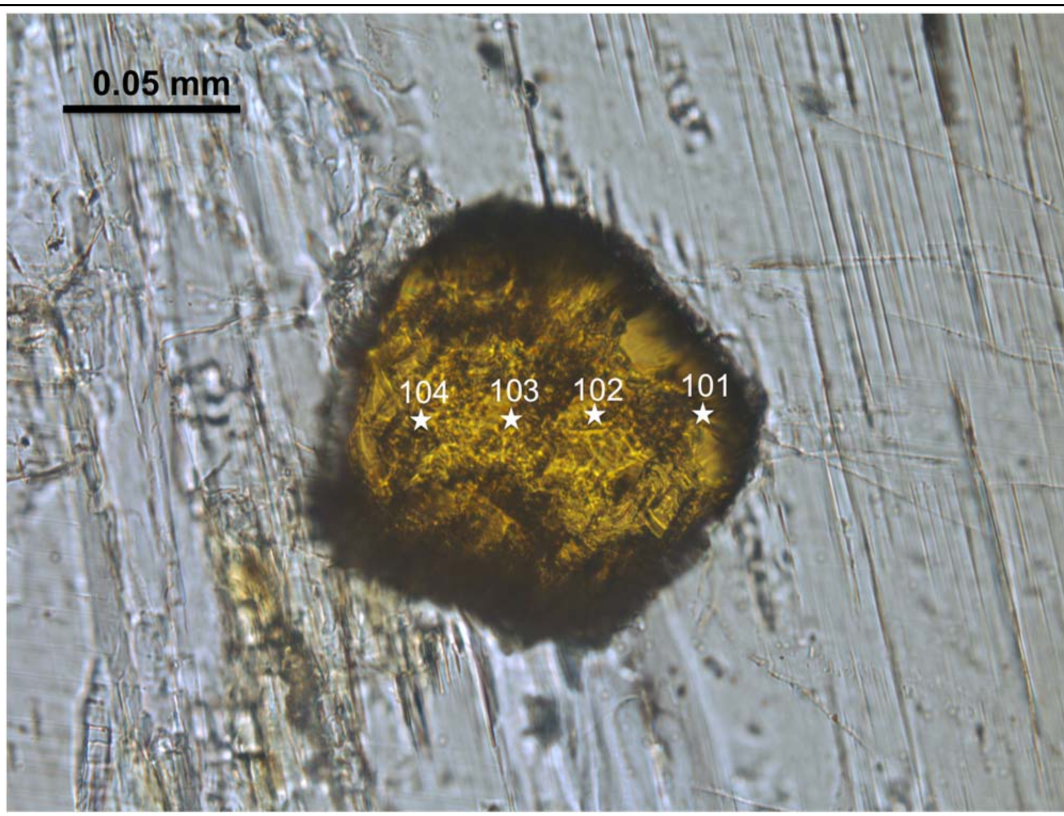

Figure 22: Rutile grain #1 from actinolite schist rind (A10-3a). Stars denote EPMA run number.

Appendix C: Actinolite Schist Rind

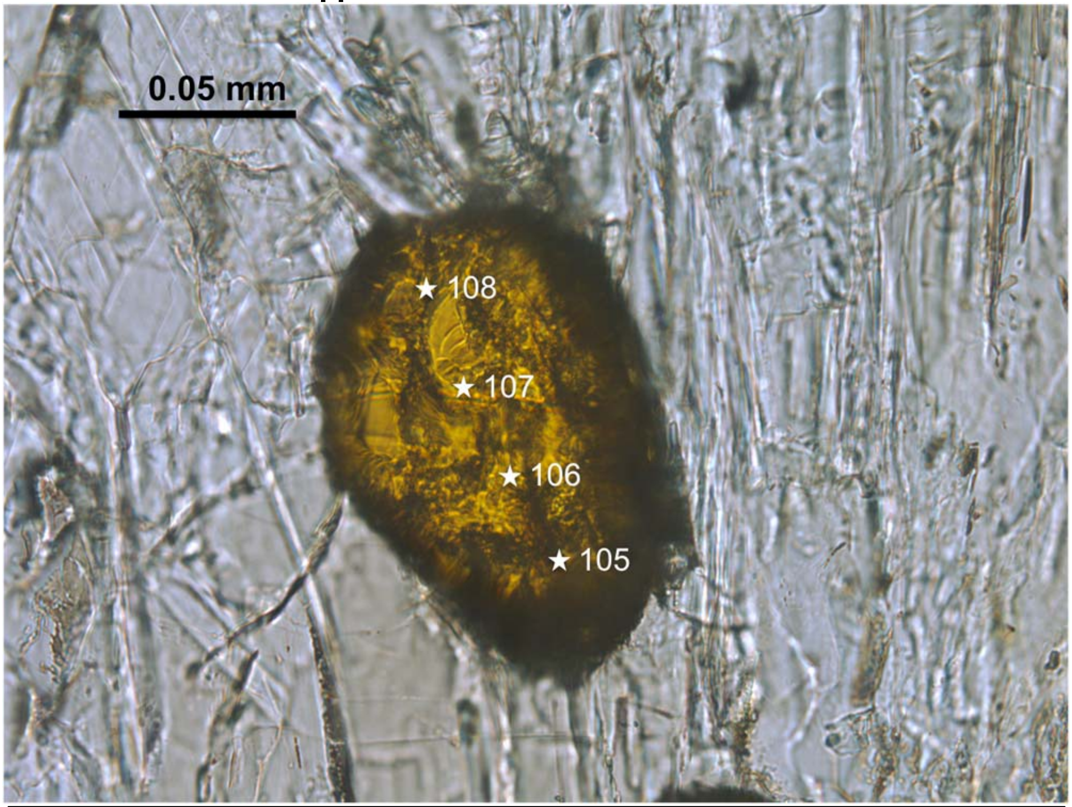

Figure 23: Rutile grain #2 from actinolite schist rind (A10-3a). Stars denote EPMA run number.

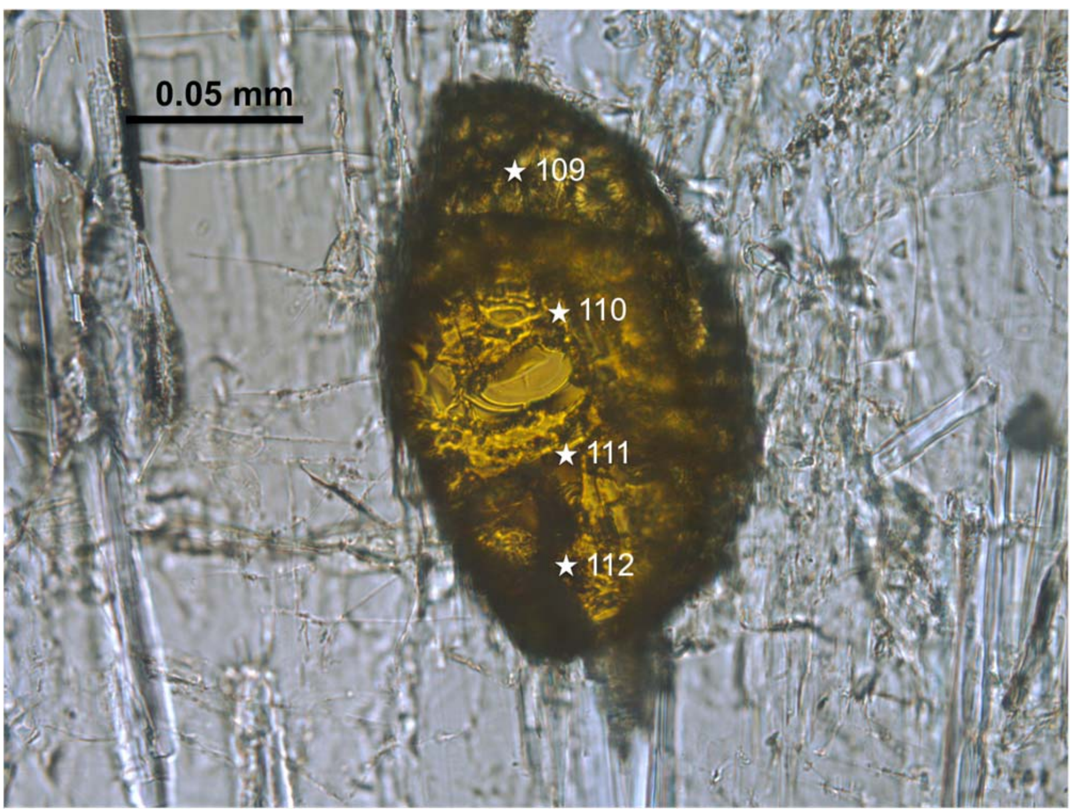

Figure 24: Rutile grain #3 from actinolite schist rind (A10-3a). Stars denote EPMA run number.

Appendix C: Actinolite Schist Rind

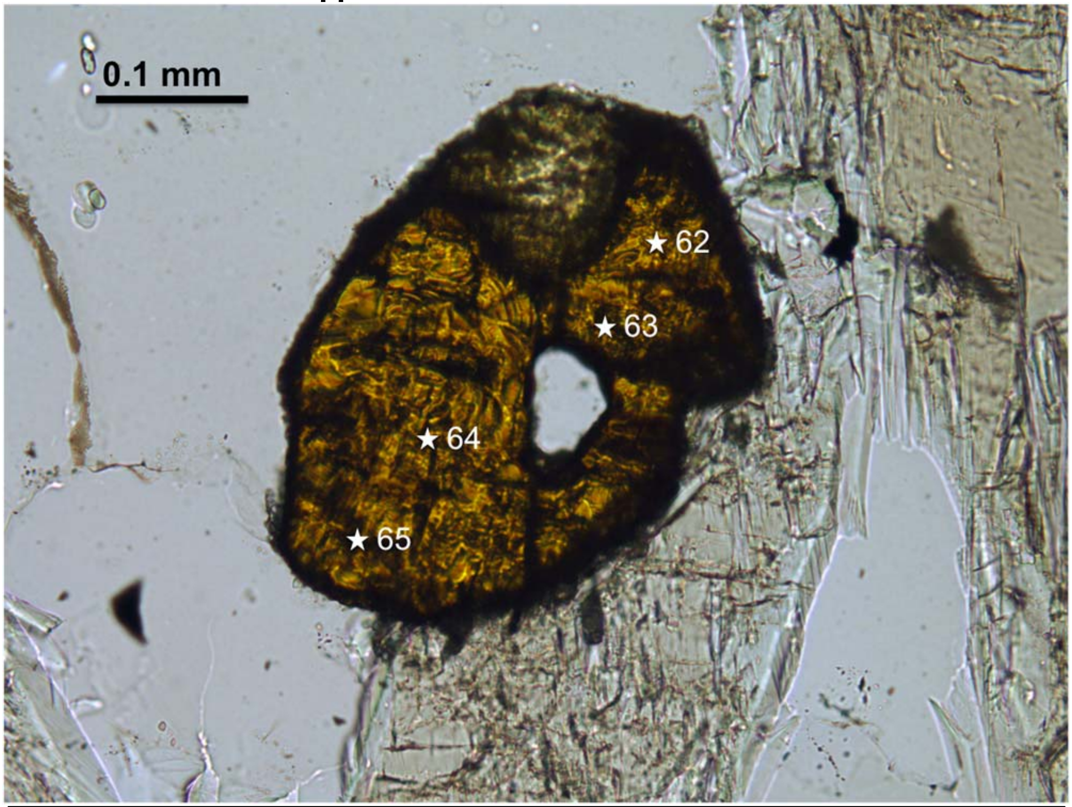

Figure 25: Rutile grain #4 from actinolite schist rind (A10-3a). Stars denote EPMA run number.

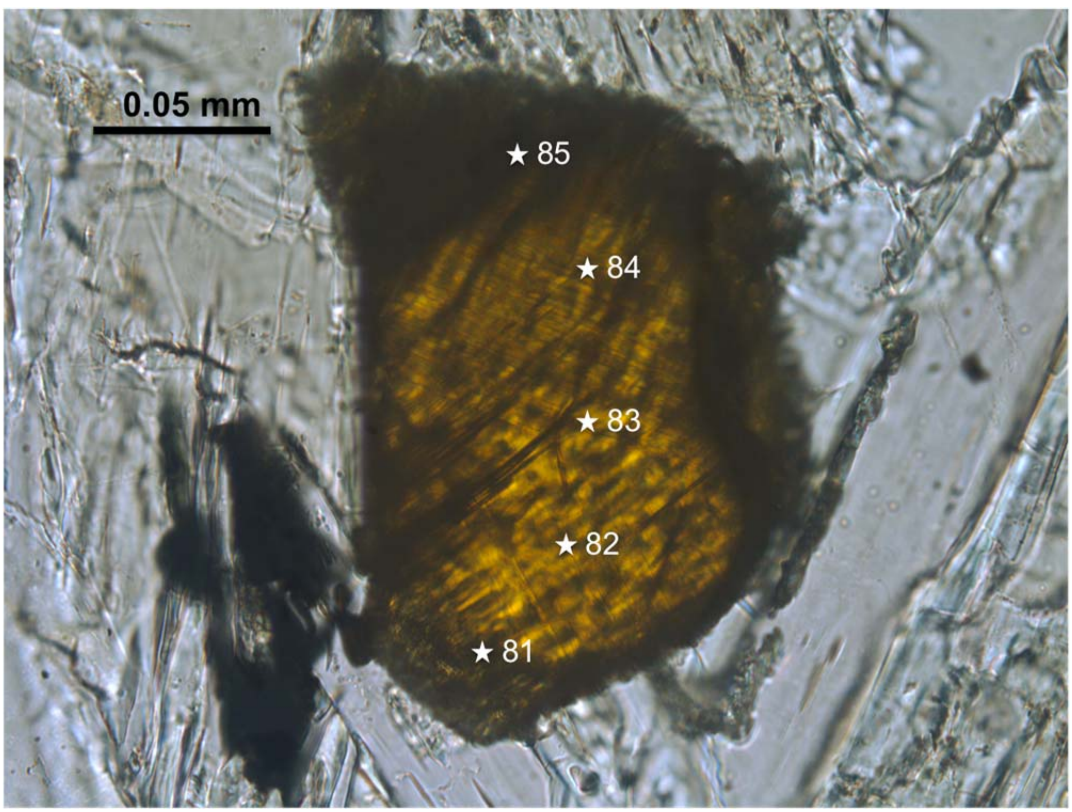

Figure 26: Rutile grain #5 from actinolite schist rind (A10-3a). Stars denote EPMA run number.

Appendix C: Actinolite Schist Rind

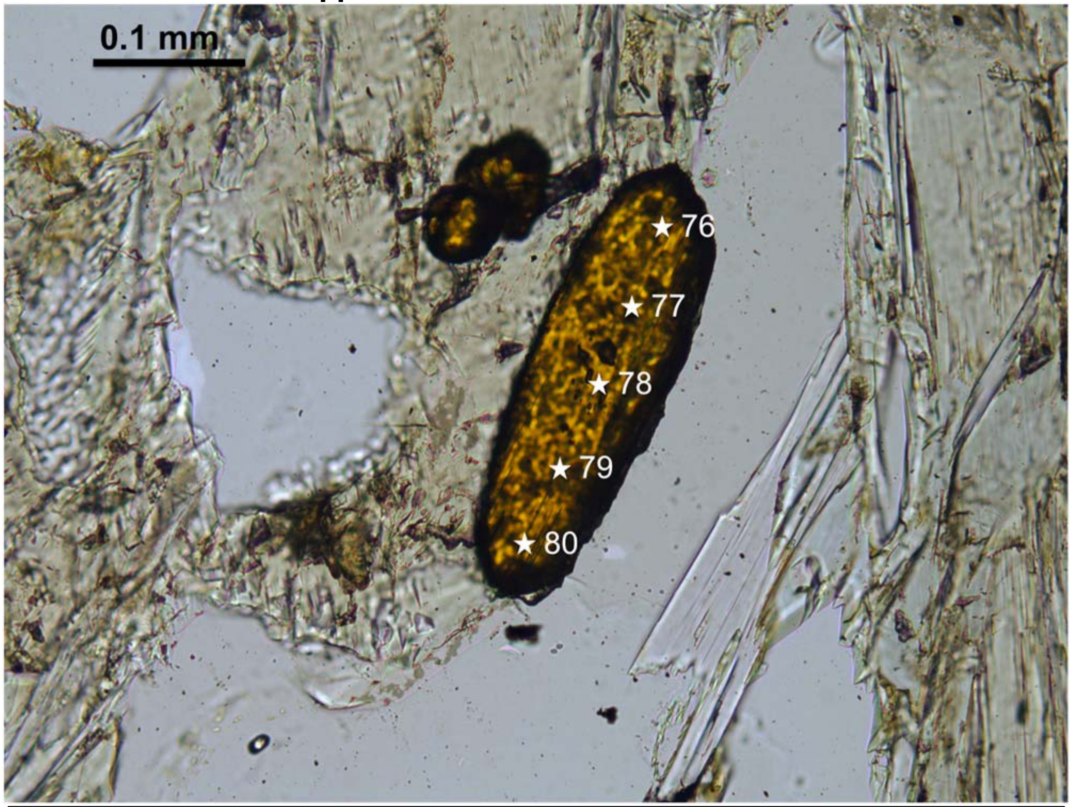

Figure 27: Rutile grain #7 from actinolite schist rind (A10-3a). Stars denote EPMA run number.

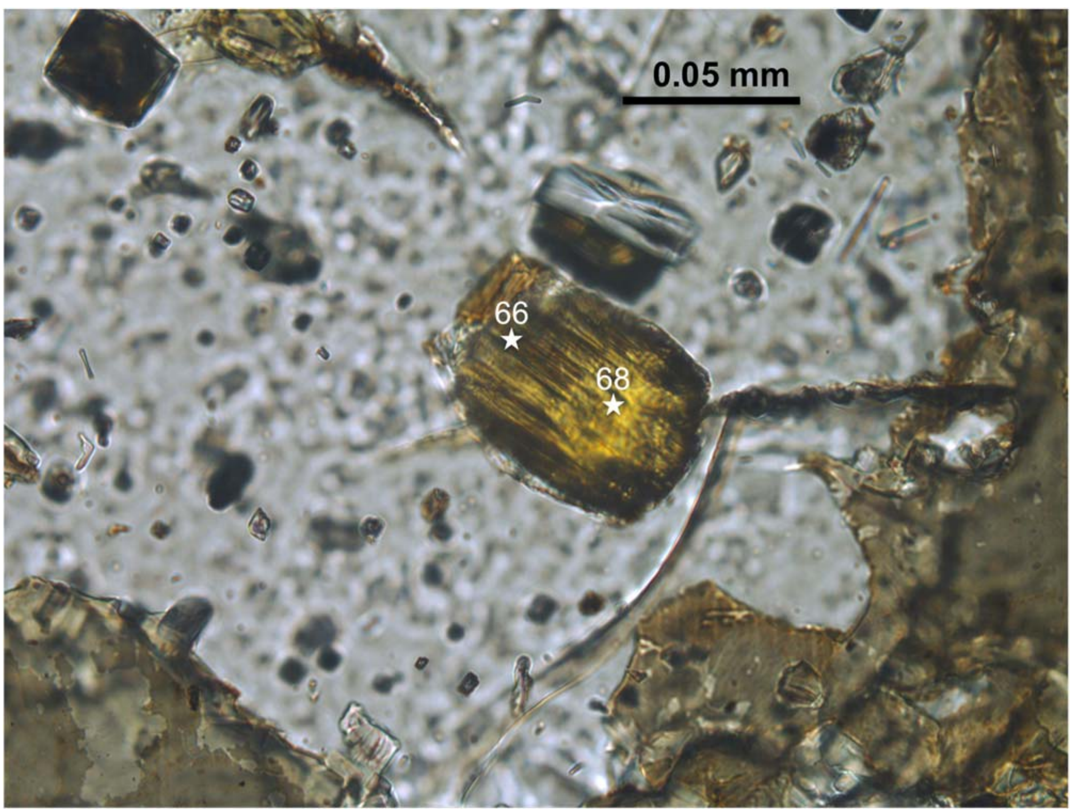

Figure 28: Rutile grain #8 from actinolite schist rind (A10-3a). Stars denote EPMA run number.

Appendix C: Actinolite Schist Rind

Figure 29: Rutile grain #9 from actinolite schist rind (A10-3a). Stars denote EPMA run number.

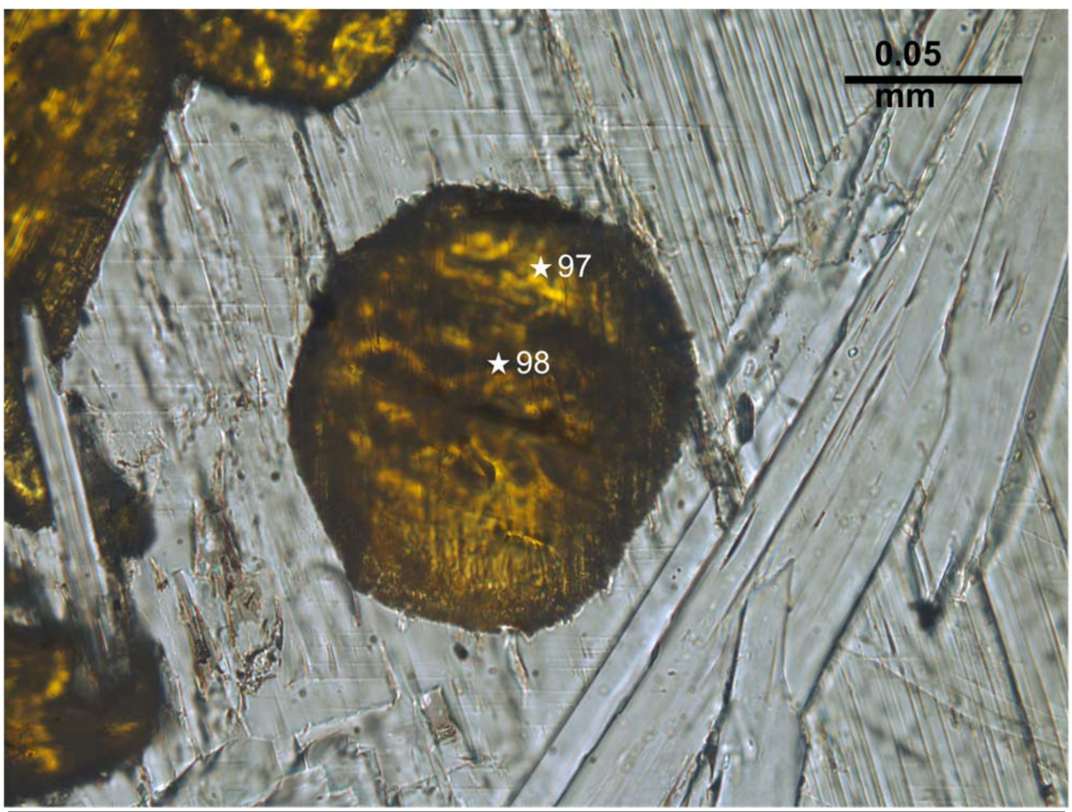

Figure 30: Rutile grain #10 from actinolite schist rind (A10-3a). Stars denote EPMA run number.

Appendix C: Actinolite Schist Rind

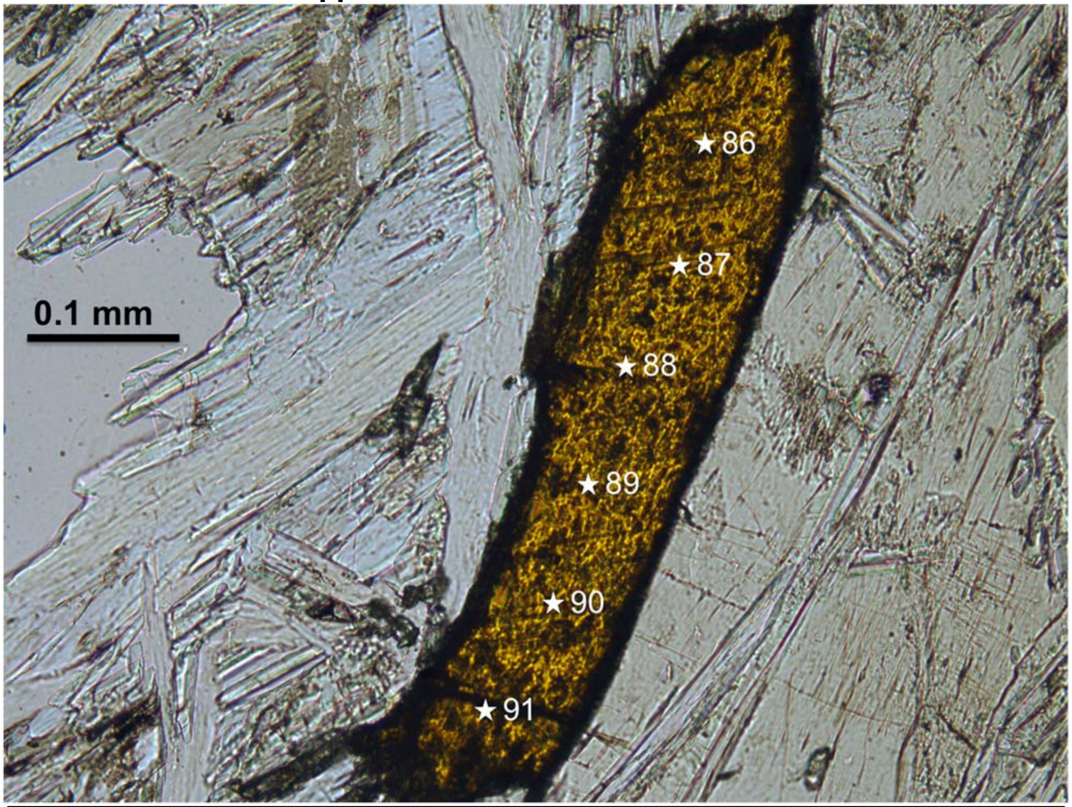

Figure 31: Rutile grain #11 from actinolite schist rind (A10-3a). Stars denote EPMA run number.

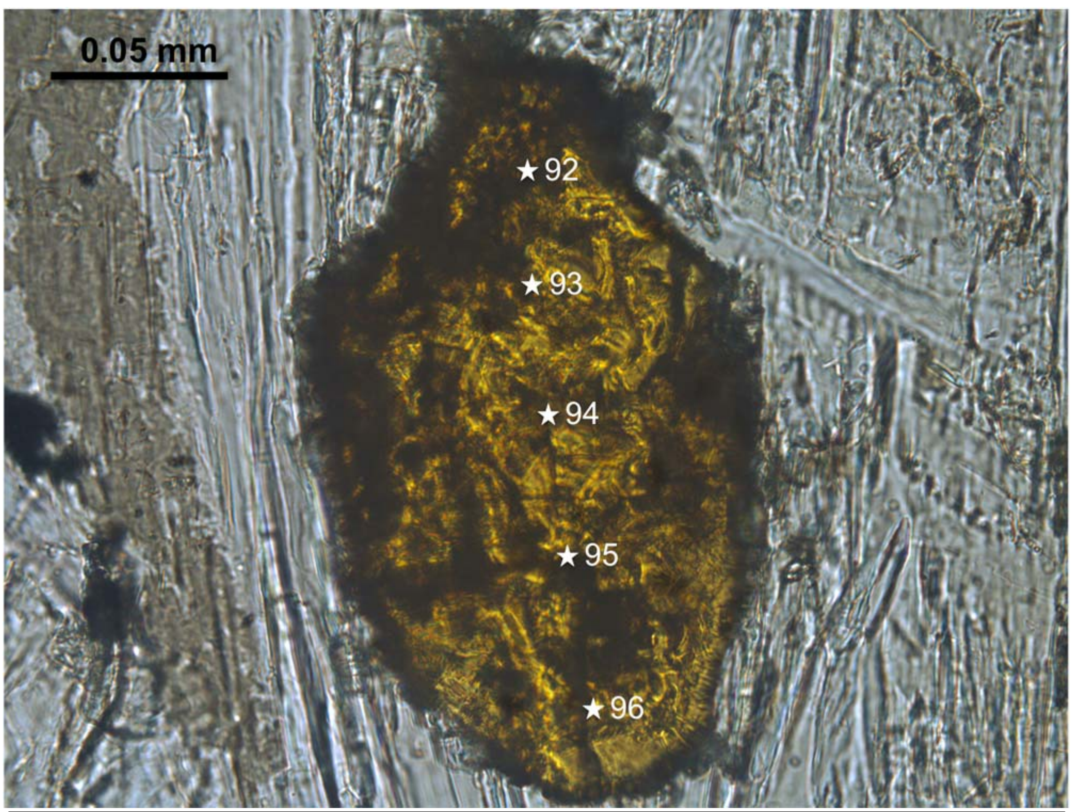

Figure 32: Rutile grain #12 from actinolite schist rind (A10-3a). Stars denote EPMA run number.

Appendix D: Garnet Quartzite

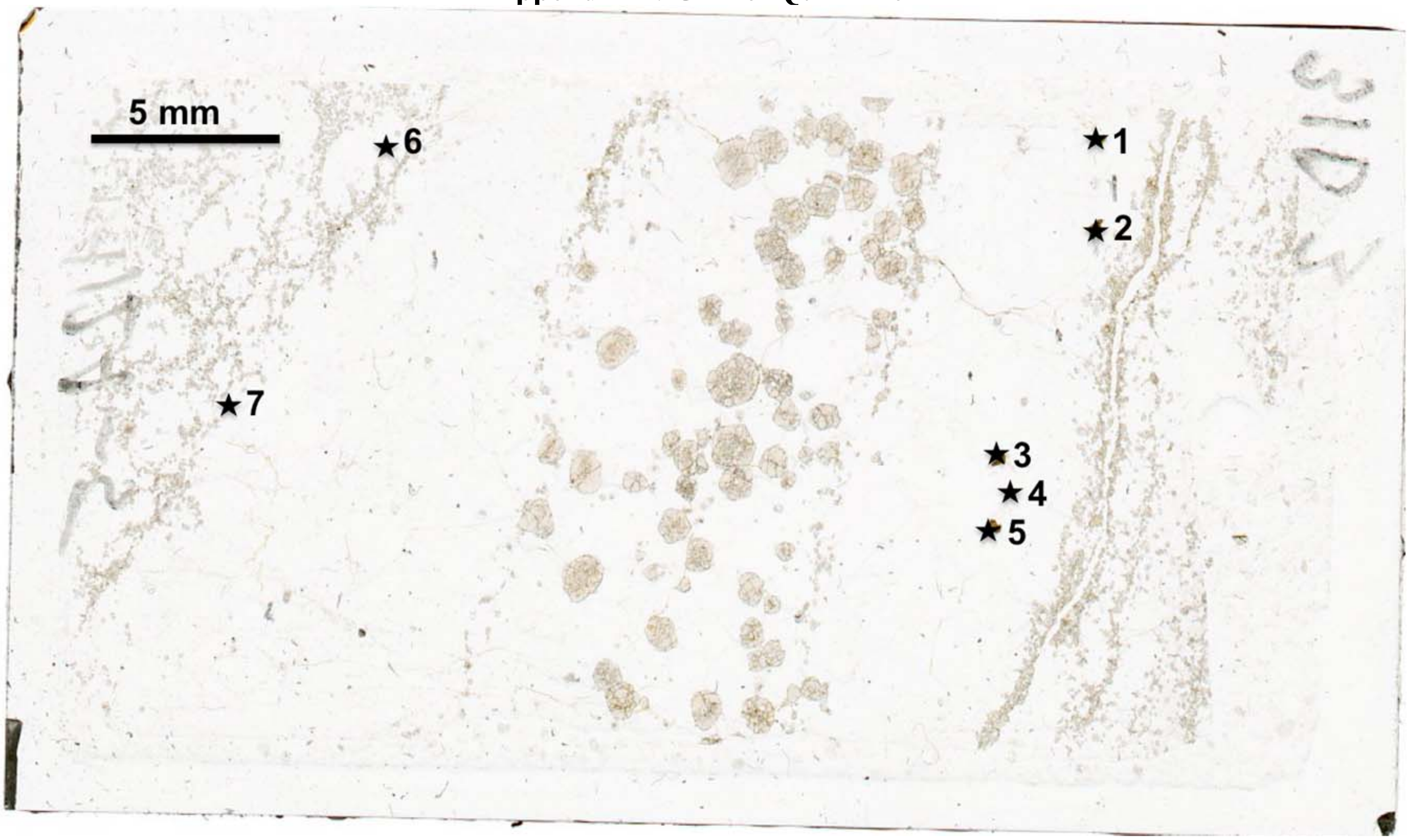

Figure 33: Thin section map of garnet quartzite (A12A-5) showing location of the seven rutile grains analyzed as denoted by stars. Numbers denote grain number, and correspond to grain number in tables 3 and 4, as well grain number in the following photomicrographs.

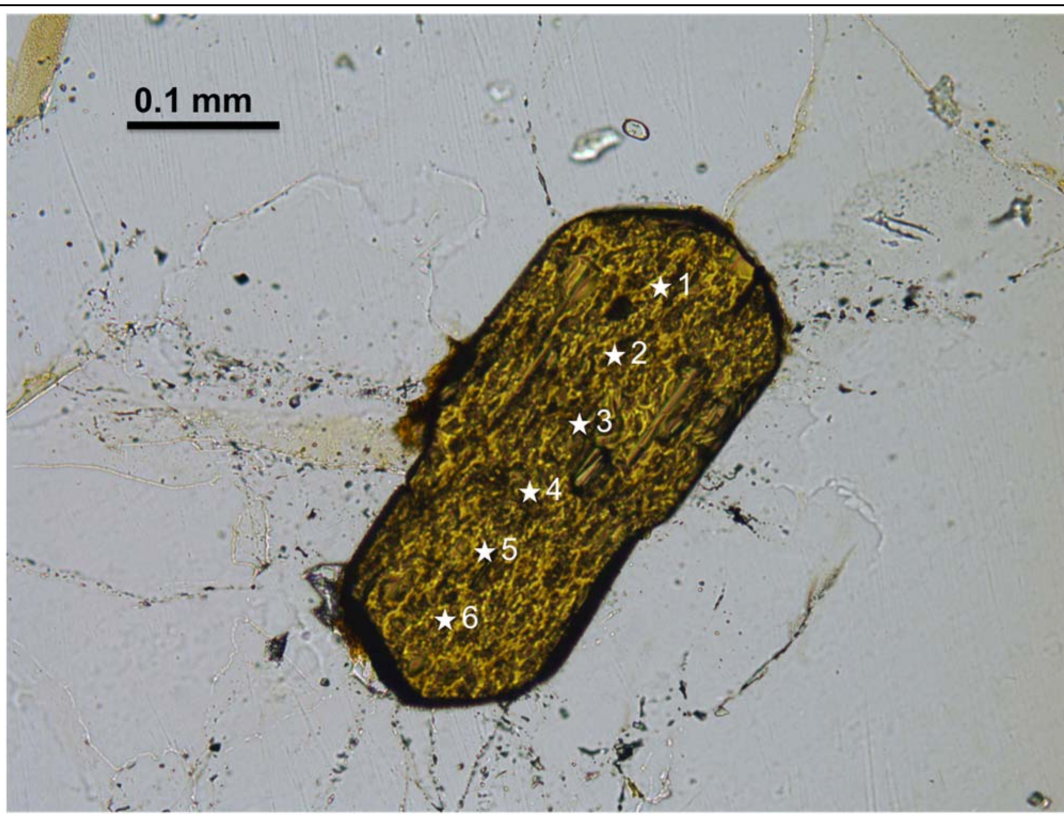

Figure 34: Rutile grain #1 from garnet quartzite (A12A-5). Stars denote EPMA run number.

Appendix D: Garnet Quartzite

Figure 35: Rutile grain #2 from garnet quartzite (A12A-5). Stars denote EPMA run number.

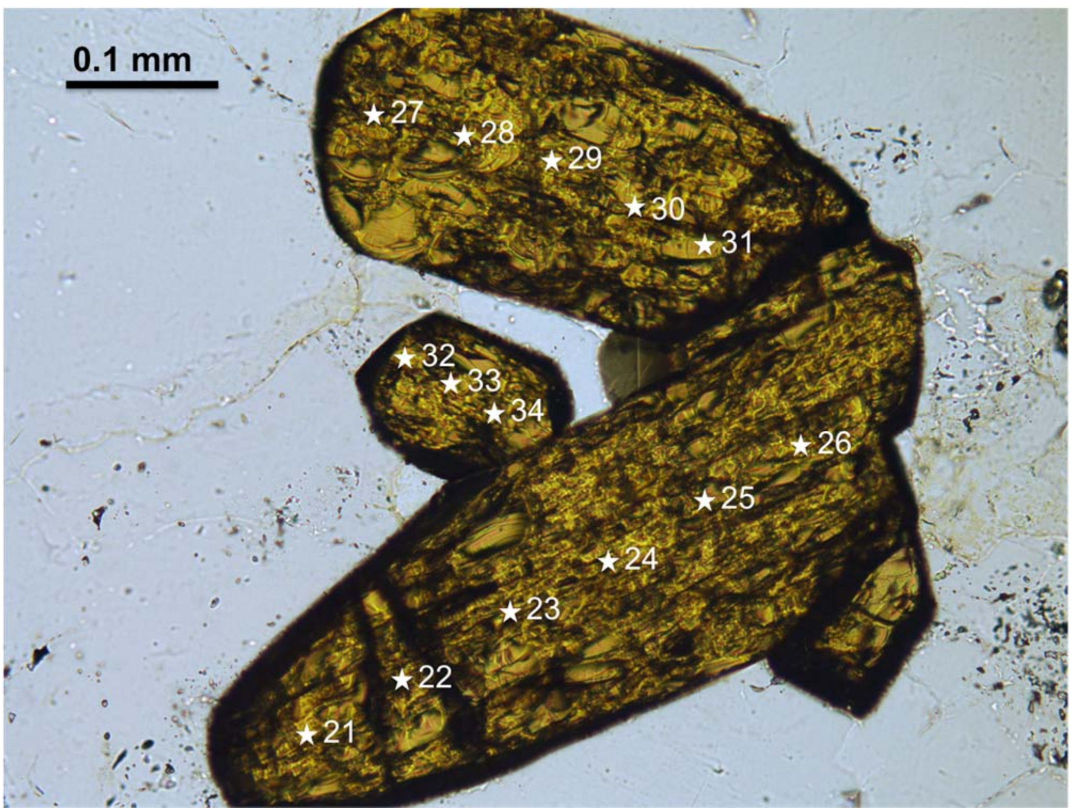

Figure 36: Rutile grain #3 from garnet quartzite (A12A-5). Stars denote EPMA run number.

Appendix D: Garnet Quartzite

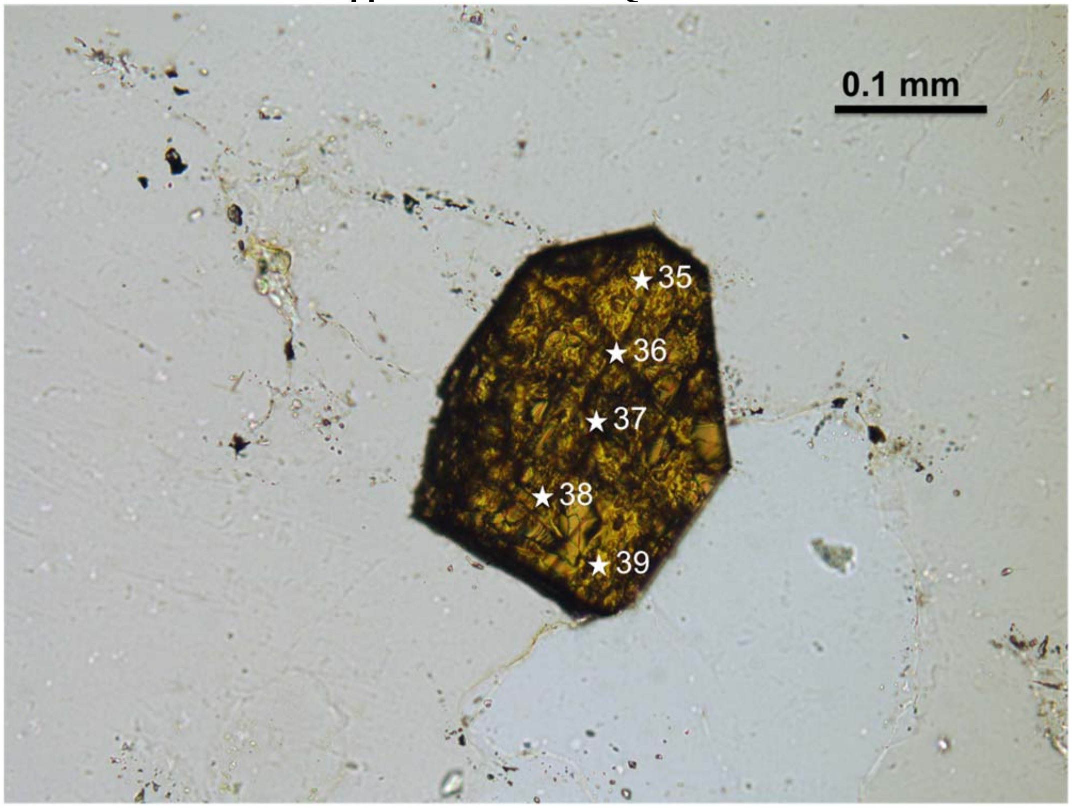

Figure 37: Rutile grain #4 from garnet quartzite (A12A-5). Stars denote EPMA run number.

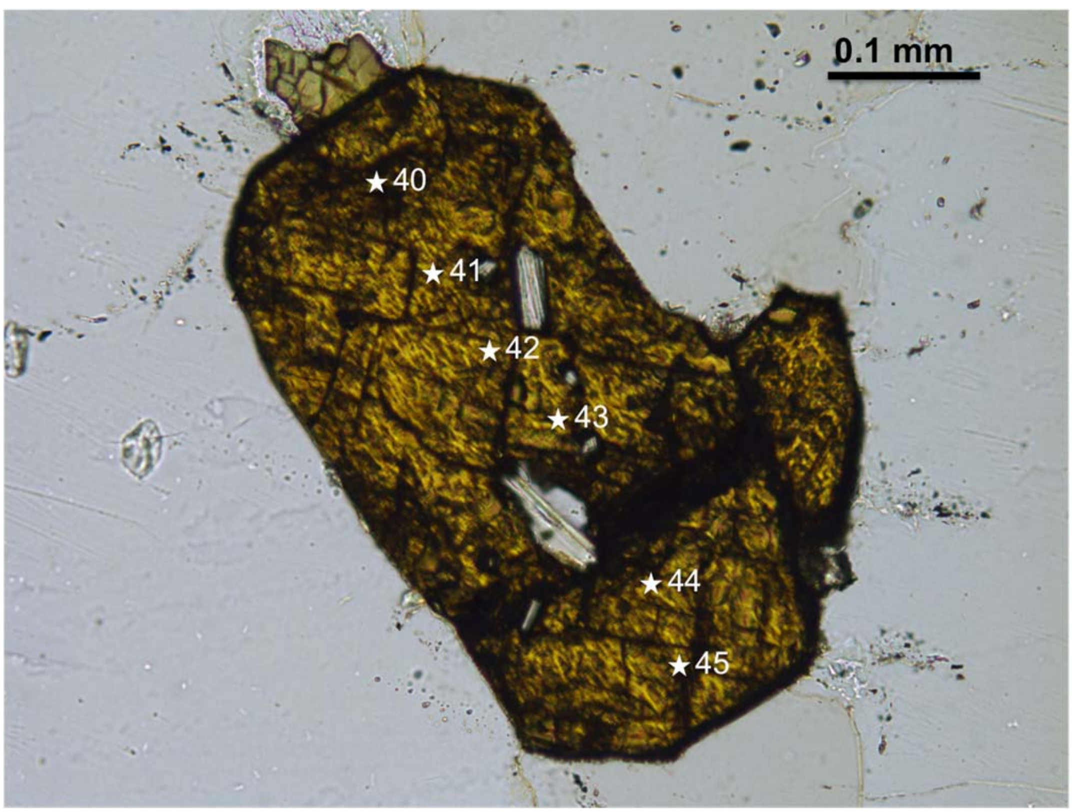

Figure 38: Rutile grain #5 from garnet quartzite (A12A-5). Stars denote EPMA run number.

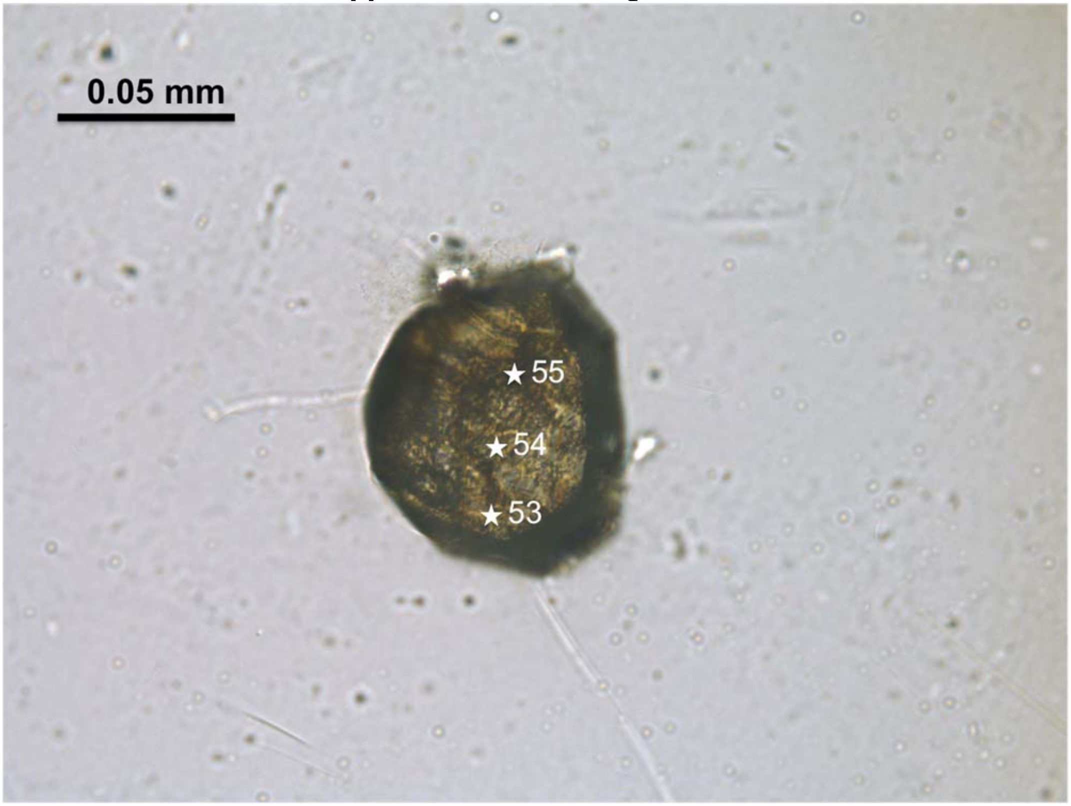

Figure 39: Rutile grain #6 from garnet quartzite (A12A-5). Stars denote EPMA run number.

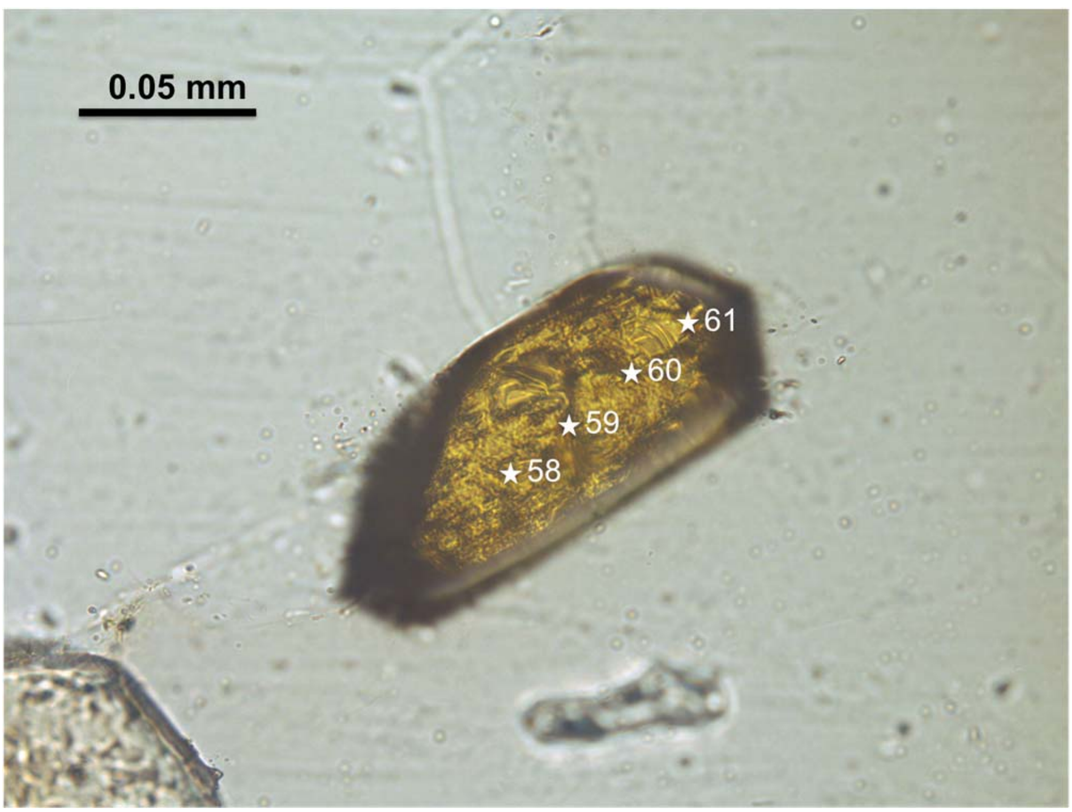

Figure 40: Rutile grain #7 from garnet quartzite (A12A-5). Stars denote EPMA run number.

Appendix E: Garnet Blueschist

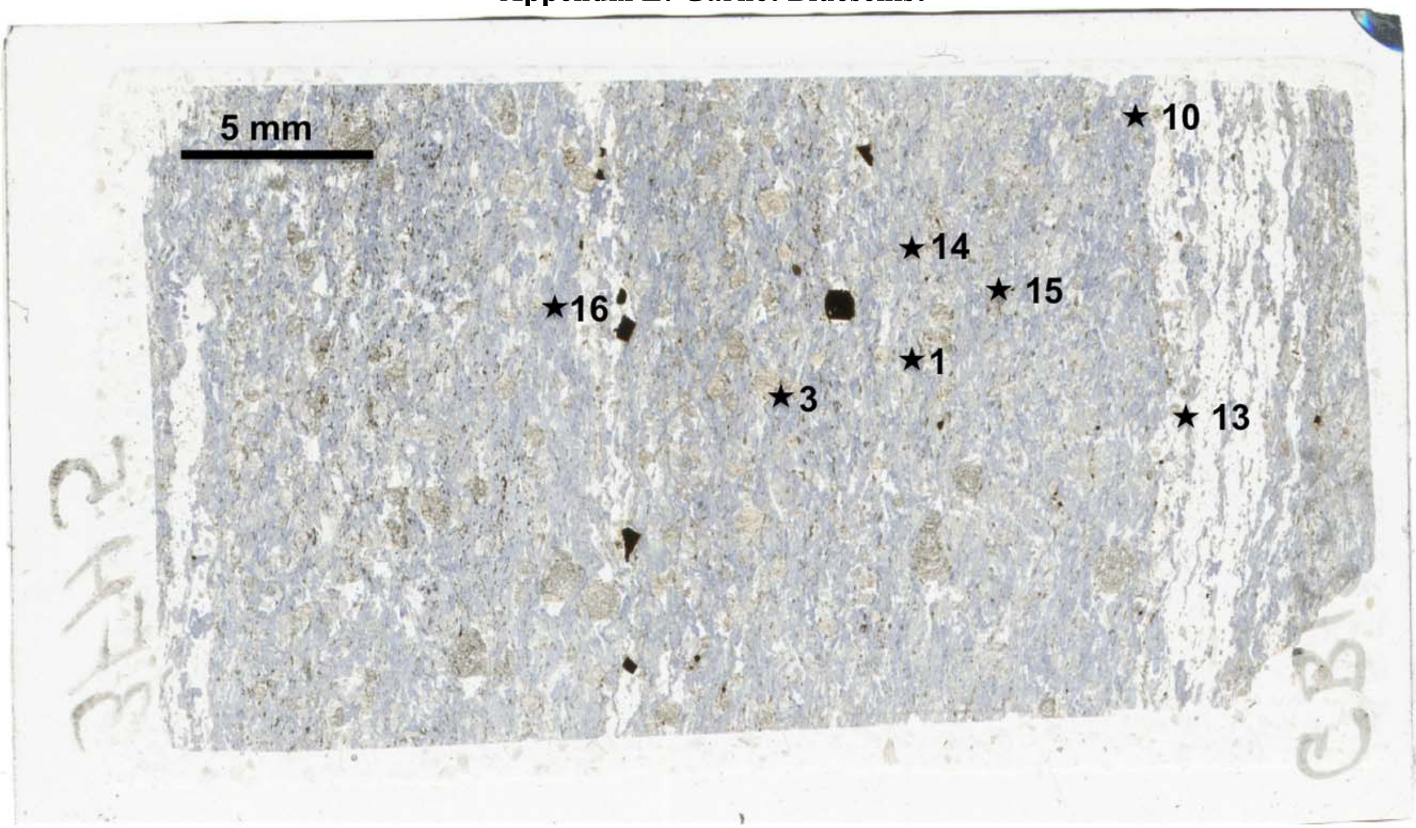

Figure 41: Thin section map of garnet blueschist (GB12-1a) showing location of the seven rutile grains analyzed as denoted by stars. Numbers denote grain number, and correspond to grain number in tables 3 and 4, as well grain number in the following photomicrographs.

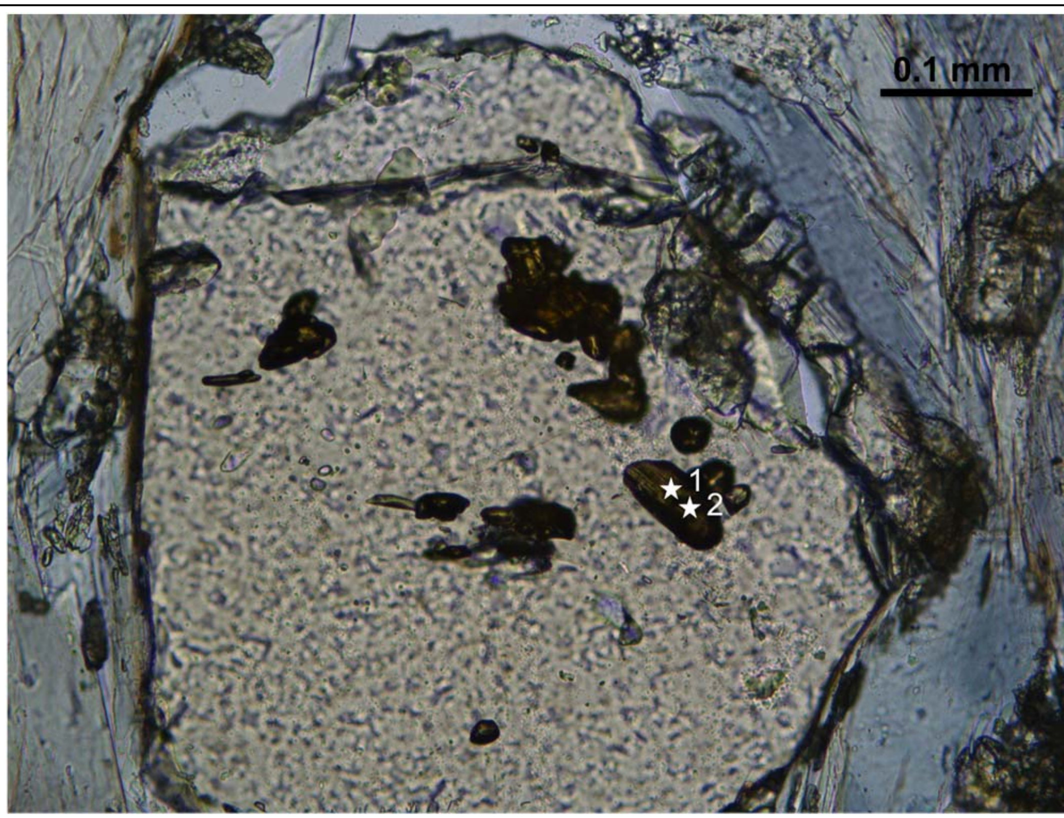

Figure 42: Rutile grain #1 from garnet blueschist (GB12-1a). Stars denote EPMA run number.

Appendix E: Garnet Blueschist

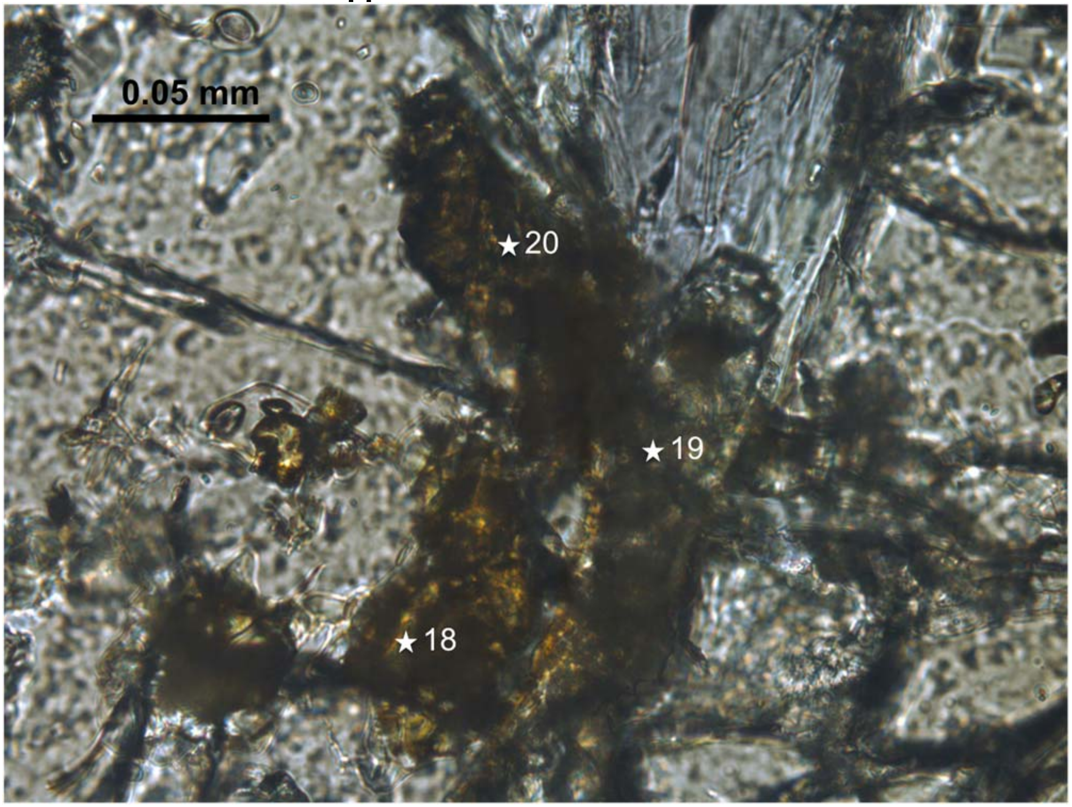

Figure 43: Rutile grain #3 from garnet blueschist (GB12-1a). Stars denote EPMA run number.

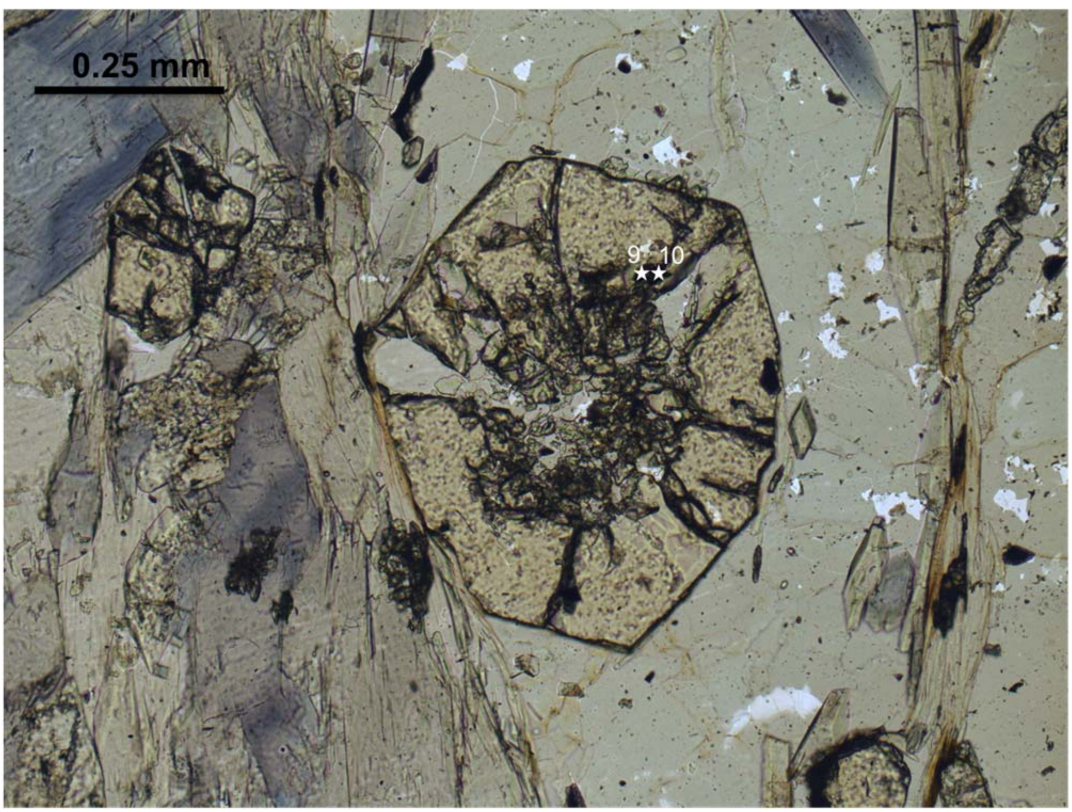

Figure 44: Rutile grain #10 from garnet blueschist (GB12-1a). Stars denote EPMA run number.

Appendix E: Garnet Blueschist

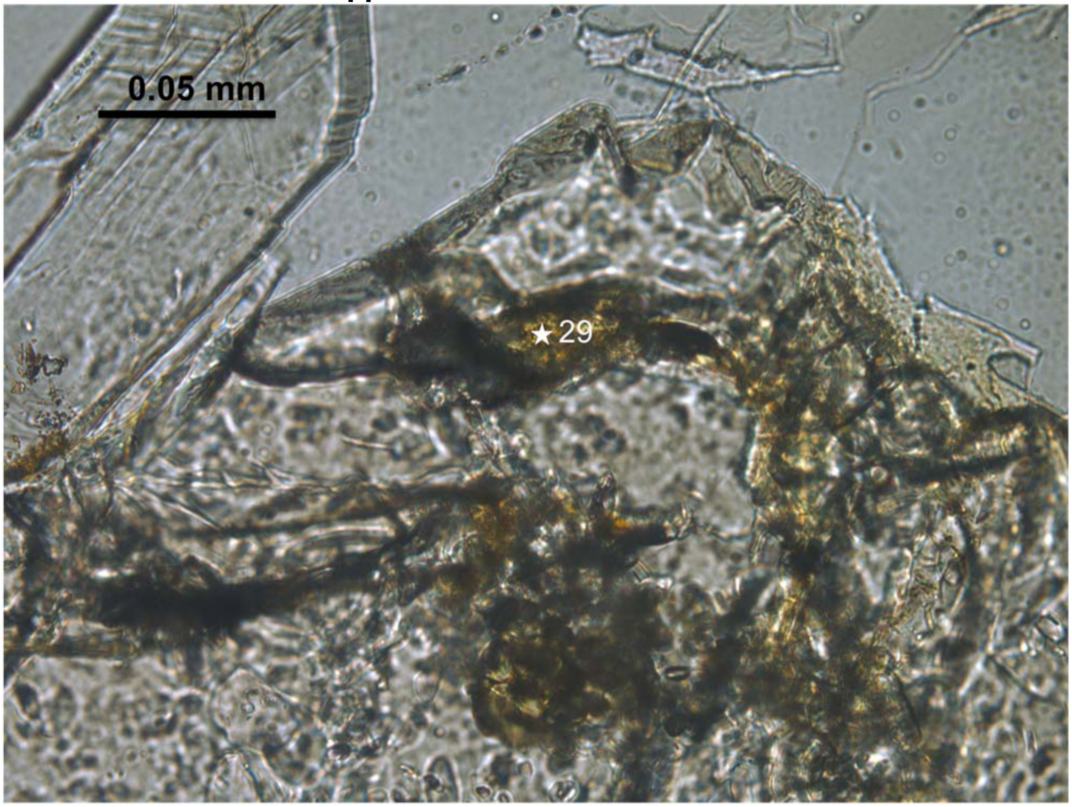

Figure 45: Rutile grain #13 from garnet blueschist (GB12-1a). Star denotes EPMA run number.

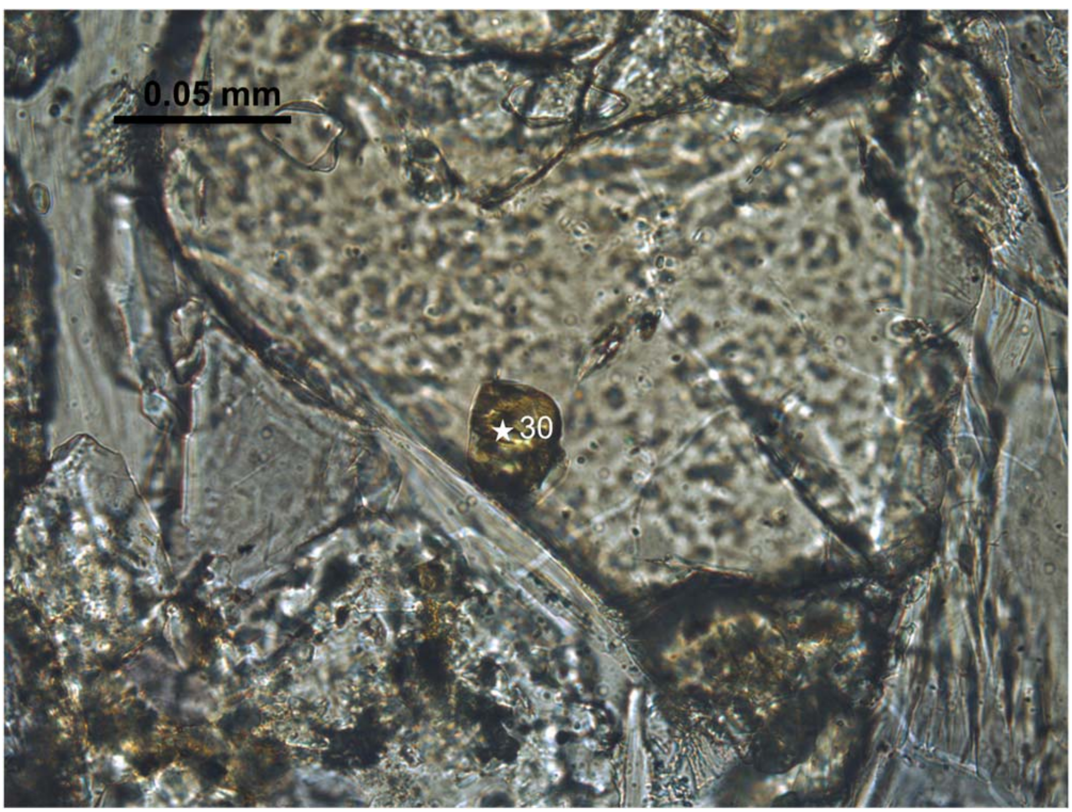

Figure 46: Rutile grain #14 from garnet blueschist (GB12-1a). Star denotes EPMA run number.

Appendix E: Garnet Blueschist

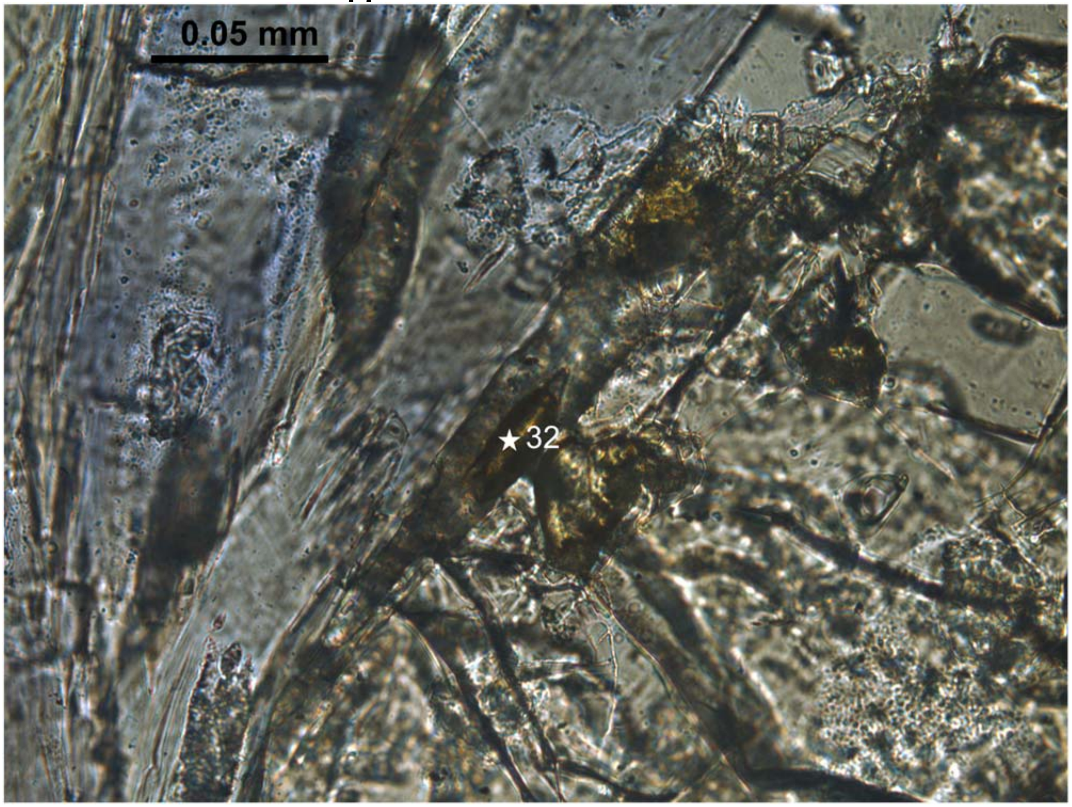

Figure 47: Rutile grain #15 from garnet blueschist (GB12-1a). Star denotes EPMA run number.

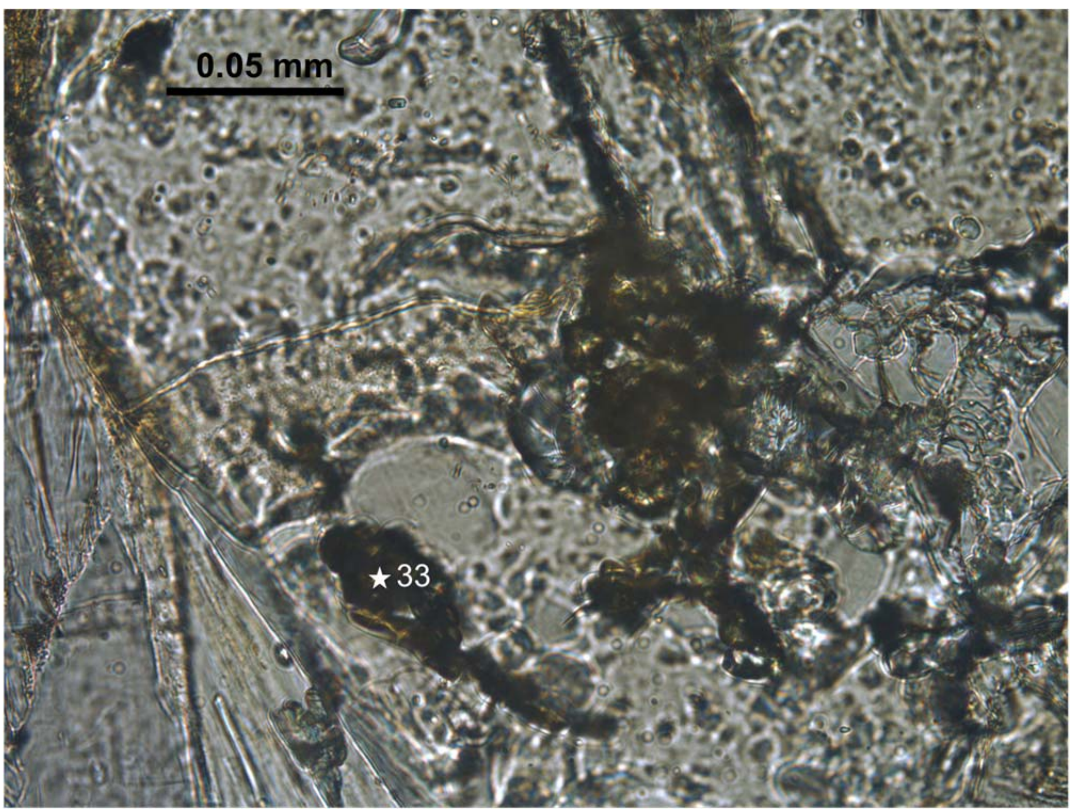

Figure 48: Rutile grain #16 from garnet blueschist (GB12-1a). Star denotes EPMA run number.